COLLÈGE DE FRANCE
1530

Chaire de Physique
de la Matière Condensée
Antoine Georges

Contrôle des fonctionnalités des oxydes

Hétéro-structures, Impulsions Lumineuses

Cours 2 – Oxydes, Interfaces et Hétérostructures: de la structure à la structure électronique

Cycle 2016-2017
2 mai 2017

Chaire de Physique
de la Matière Condensée
Antoine Georges

Control of oxide functionalities:

Heterostructures, Light pulses

Lecture 2 – Oxides, interfaces and heterostructures: from structure to electronic structure

Most slides will be in English

2016-2017 Lectures
May 2, 2017

Lecture 1 (overview/summary)

- Strain – control of oxide functionalities.
- Carrier density control by gating/ionic liquids → more examples in online slides or end of this lecture, time permitting.
- Engineering a new functionality by combining two (or more) materials → see later in this lecture
- Creating 2D electron gases/liquids at oxide interfaces (e.g. LAO/STO with nominal carrier density up to 3.10^{14} cm^{-2}).

Today's Lecture:

Basic notions about the structure and electronic structure of oxides

(with thin films and heterostructures in mind)

Today's seminar – May 2nd

Alexandre Gloter et Odile Stephan
LPS-Orsay

Explorer la physique aux interfaces d'oxydes fortement corrélés: résultats récents et perspectives en microscopie électronique.

https://www.stem.lps.u-psud.fr

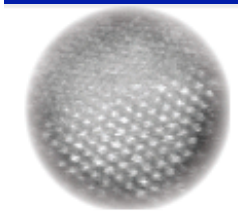

STEM@LPS

The stem group at the laboratoire de physique des solides

Search

Home | Research | News | People | Equipement | Publications | Jobs | Images | Teaching

- Login
- Register

La microscopie electronique

a book of
Christian Colliex

The STEM Group is a french world leading electron microscopy group, specialising in electron energy loss spectroscopy (EELS). Our scientific interests are large, and are including different parts of the physics and material sciences: nanoparticles, interfaces, nanophotonic... We are constantly developing instrumentation and methods in the fields of electron microscopies and spectroscopies.

Recent Research Highlights

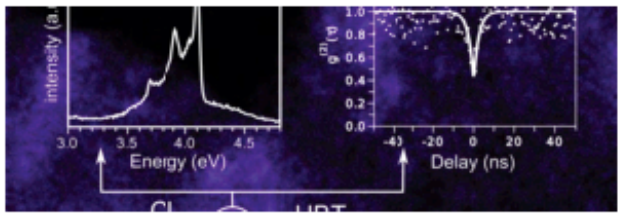

Point Defects in h-BN as efficient UV quantum emitters

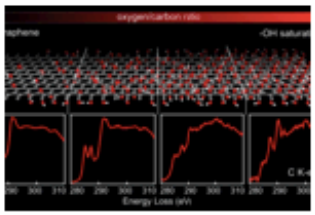

Revisiting Graphene Oxide Chemistry

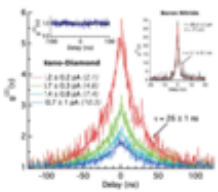

Photon Bunching in Cathodoluminescence

Nanometric resolved luminescence in h-BN Flakes: excitons and stacking order

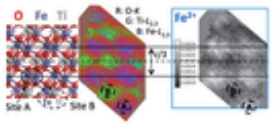

Direct Evidence of Fe2+/Fe3+ Charge Ordering in the Ferrimagnetic Hematite-Ilmenite Fe1.35Ti0.65O3-d Thin Films

Tweets by @STEM_LPS

STEM_LPS
@STEM_LPS

1. Crystal structures
- Mostly perovskites -

Periodic Table of the Elements

Transition Metals

→ 3d transition metals

→ 4d transition metals

→ 5d transition metals

Rare earths and Actinides

Lanthanide Series*	58 Ce	59 Pr	60 Nd	61 Pm	62 Sm	63 Eu	64 Gd	65 Tb	66 Dy	67 Ho	68 Er	69 Tm	70 Yb	71 Lu
Actinide Series~	90 Th	91 Pa	92 U	93 Np	94 Pu	95 Am	96 Cm	97 Bk	98 Cf	99 Es	100 Fm	101 Md	102 No	103 Lr

Electronic configuration of neutral isolated atom:

Structures

2.1 Monoxides **MO**: <u>not much controllability…</u>

NaCl structure

Nominal valences:
(quite ionic)
- Oxygen takes 2 electrons
→ Ligand shell $2s^2 2p^6$ full
- M gives out two electrons:
→ M^{2+}

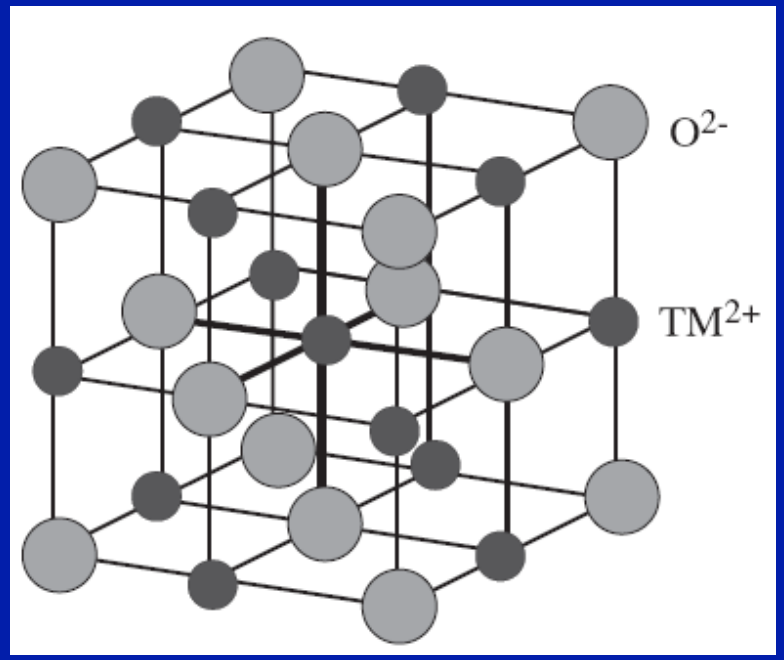

TiO, VO: ~ metals
(O-deficient)

MnO, CoO, NiO: Mott
(or charge-transfer)
magnetic insulators
(historic example: NiO)

Oxide	Electronic Configuration O^{2-}	Electronic Configuration TM^{2+}	Insulating gap (eV)	Néel Temperature (K)
MnO	[He] $2s^2 2p^6$	[Ar] $3d^5$	3.6–4.2[a]	118[d]
CoO	[He] $2s^2 2p^6$	[Ar] $3d^7$	2.5–6[b]	289[d]
NiO	[He] $2s^2 2p^6$	[Ar] $3d^8$	3.1–4.3[c]	523[d]

Ternary compounds (and more): the simple (and beautiful) perovskite structure and its descendants…

For example: $SrVO_3$

Perfectly cubic
perovskite RMO_3 :
(often noted ABO_3)

- transition-metal Ion M at center of oxygen octahedra
→MO_6 structural units
- R+O form fcc lattice
- Rare-earth ions R form simple cubic lattice

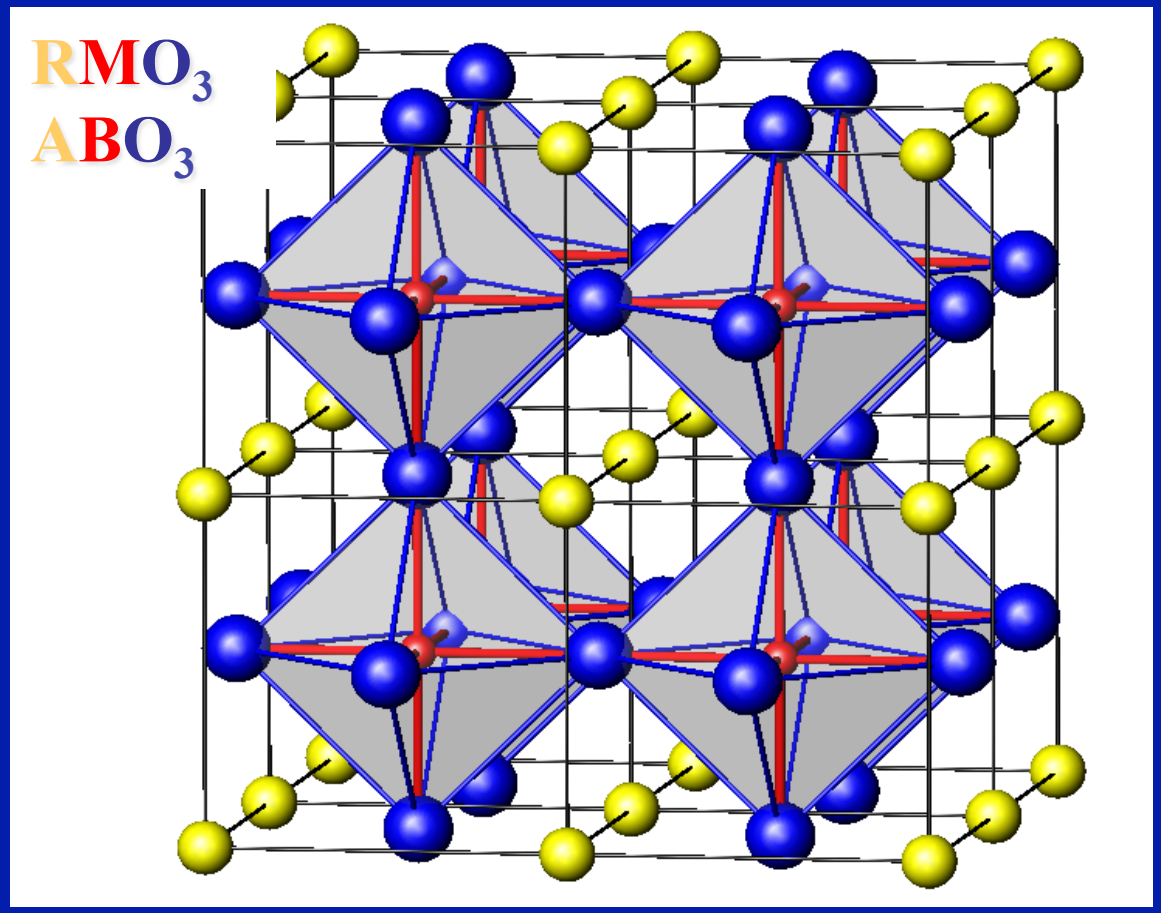

[L.A Perovski 1792-1856
Oural mountains samples
discovery of CaTiO3 G.Rose, 1839]

Perovskite: discovery and origin of the name

Count
Lev Alexeievich
Perovski
(1792-1856)
Minister of Interior
under Nicolas 1st
and Mineralogist

Gustav Rose
(1798-1873)
German mineralogist

Roselite
Armand Levy
1824

Perovskite $CaTiO_3$
described in 1839
by Gustav Rose
who named it
after Count Perovski

Perovskite: identification of crystal structure

Victor Moritz Goldschmidt
(1888 Zurich-1947 Oslo)
Pioneer of geochemistry
First described perovskite structure. Introduced `tolerance factor' and coined `lanthanide contraction' (among many achievements)
Mountain ridge Goldschmidttfjella (Spitzberg)

Helen Dick Megaw
(1907-2002)
Irish crystallographer
X-ray crystallography pioneer
Established perovskite structure
CaSnO3: Megawite
Megaw island-Antarctica (work on ice crystals)

Controlling dimensionality: the Ruddlesden-Popper series $R_{n+1}M_nO_{3n+1}$ (`layered perovskite')

Unit-cell

n=1

n=2

$Sr_3Ru_2O_7$

I4/mmm

MO_2 layer →

`single-layer ' material

MO_2 layer →

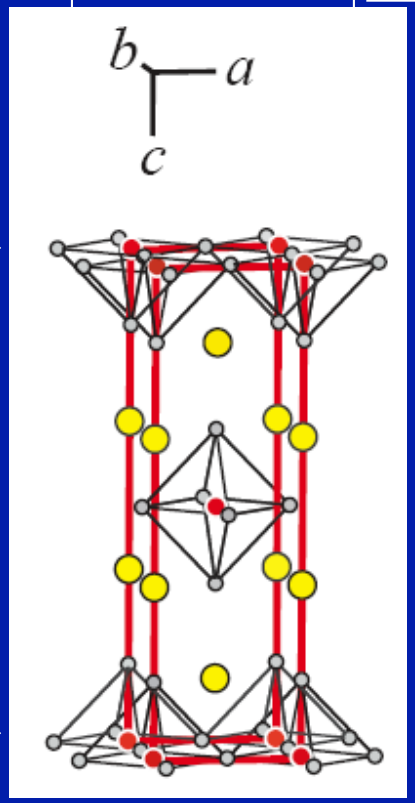

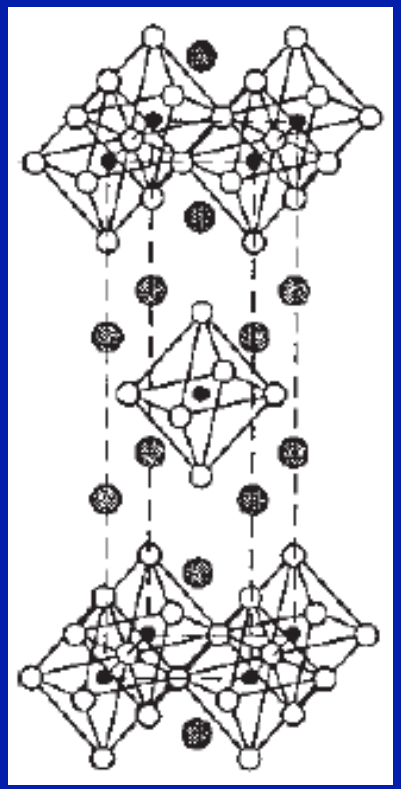

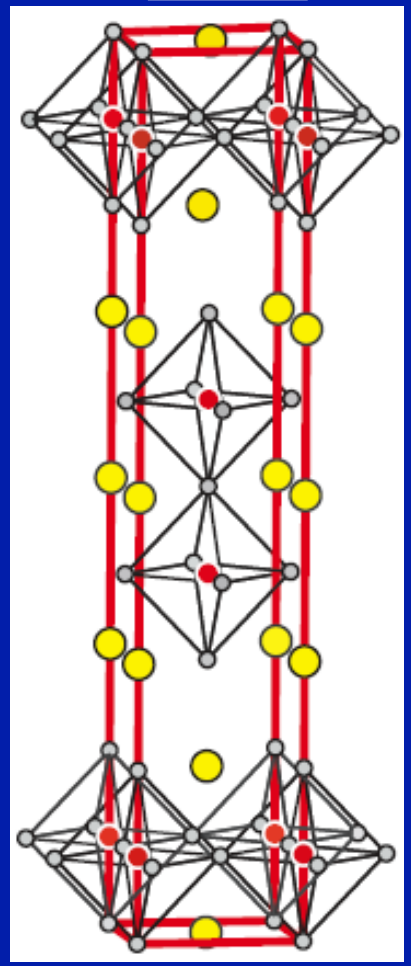

bilayer material

I4/mmm

Sr_2RuO_4

Increasing n : ``from d=2 to d=3"

Usual perovskite RMO_3 corresponds to n→infinity

Distorted perovskites

Depending on the ionic radii of the 3 ions, the material often adopts a structure which breaks perfect cubic symmetry e.g. orthorombic → See later in the lecture for more details

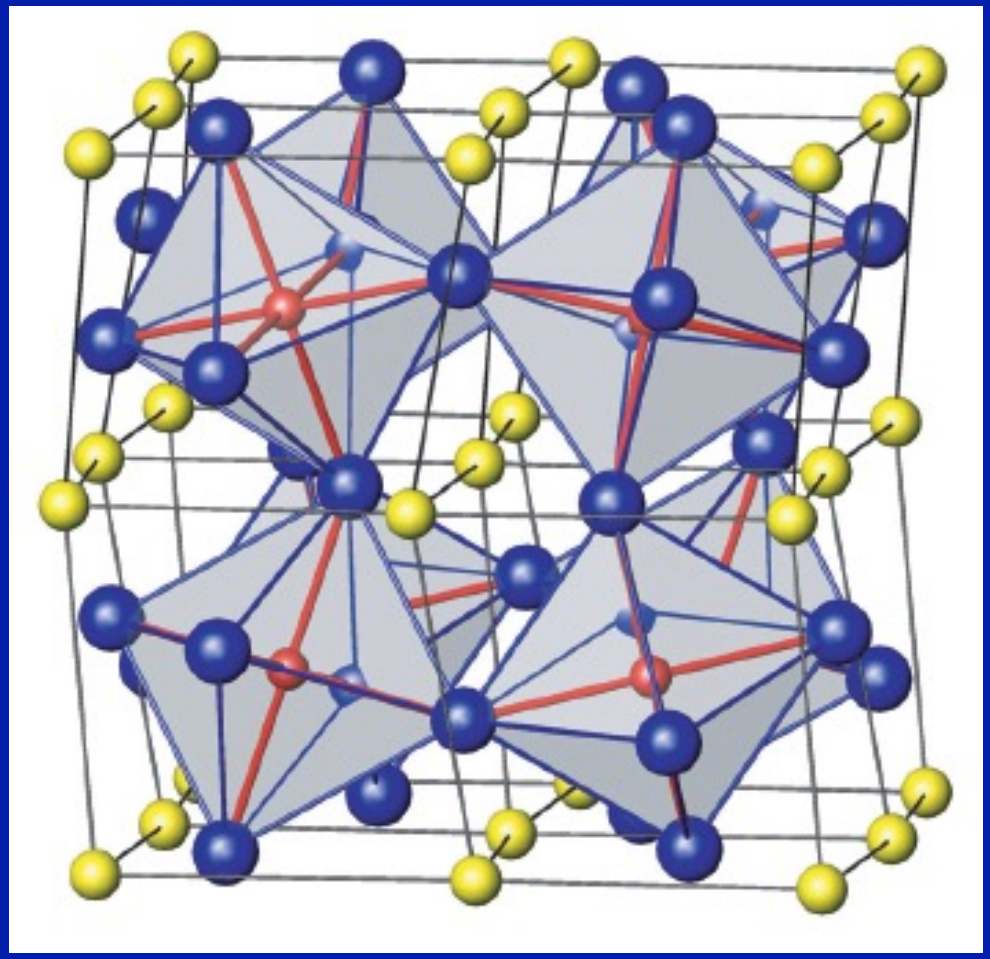

Example:
`$GdFeO_3$' distortion
- Octahedra remain perfect (no or very small Jahn-Teller)
- Rotation of octahedra along [100] = [010] and [001] a-a-c+
- Orthorombic symmetry
- 4 M-atoms per unit cell, all equivalent by symmetry
- M-O-M angle becomes π-θ

Other possible distortions
e.g rhomboedric, rotation [111]

RMO_3 : ``Tolerance factor'' (Goldschmidt)

- Consider close packing by hard spheres of radii r_R, r_M, r_O (ionic radii)
- Call `a' the lattice spacing (cubic cell)

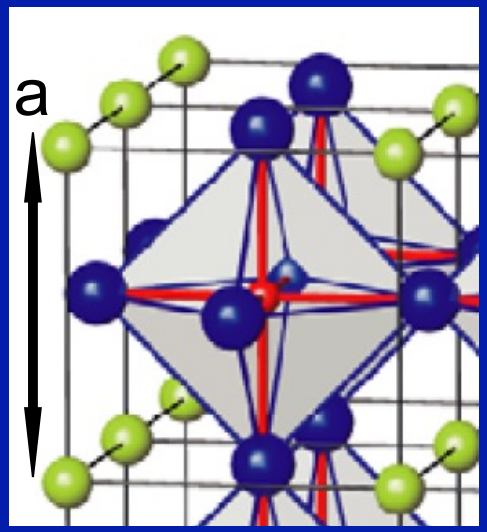

$$d(O-R) = \frac{a}{\sqrt{2}} \ , \ d(O-M) = \frac{a}{2}$$

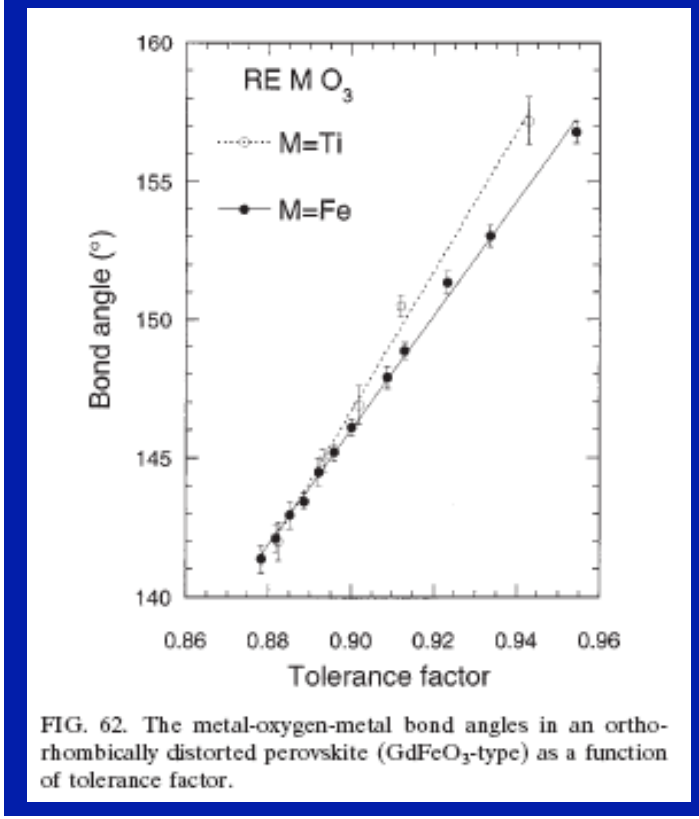

FIG. 62. The metal-oxygen-metal bond angles in an orthorhombically distorted perovskite ($GdFeO_3$-type) as a function of tolerance factor.

- Ideal packing will have:

$$t \equiv \frac{r_R + r_O}{\sqrt{2}(r_M + r_O)} = 1$$

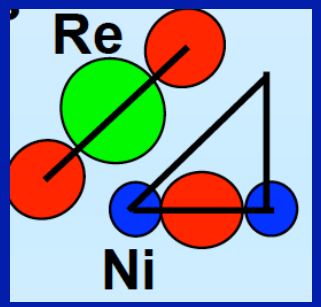

* t=1: ideal cubic perovskite
* t<1: deforms to rhomboedral, then orthorhombic
* t too small (<0.86): unstable

All this offers control on the material:

- Substitutions on R-site allow for a control of the (nominal) valence of M-ion (`doping')
- e.g: $LaTiO_3 \rightarrow La^{3+}$ [Xe], Ti^{3+} : [Ar]$3d^1$ config.
- $SrTiO_3 \rightarrow Sr^{2+}$ [Xe], Ti^{4+} : [Ar]$3d^0$ config.
- Iso-valent substitutions on R-site allow for a control of the distortion, hence of:

- Bandwidth (see below)
- And importantly of the splitting between d-levels

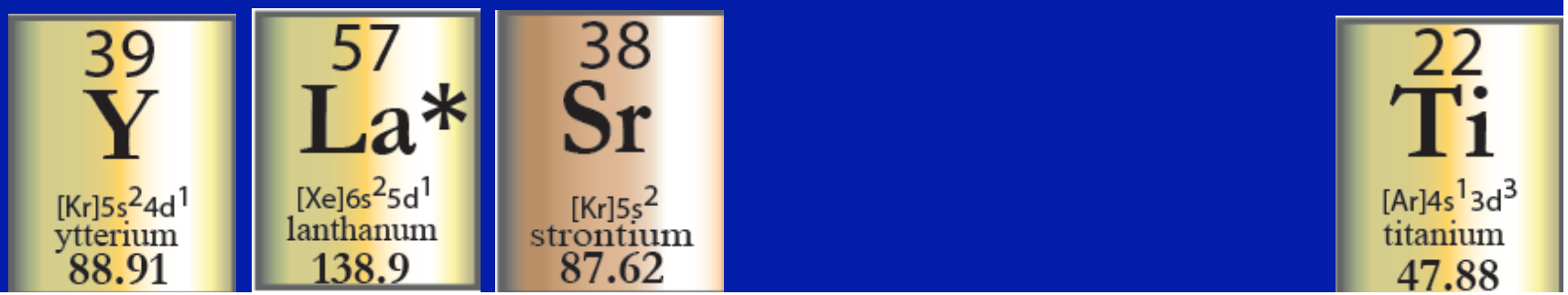

Sensitivity to distortion: $RNiO_3$ compounds (cf lectures 3-4)

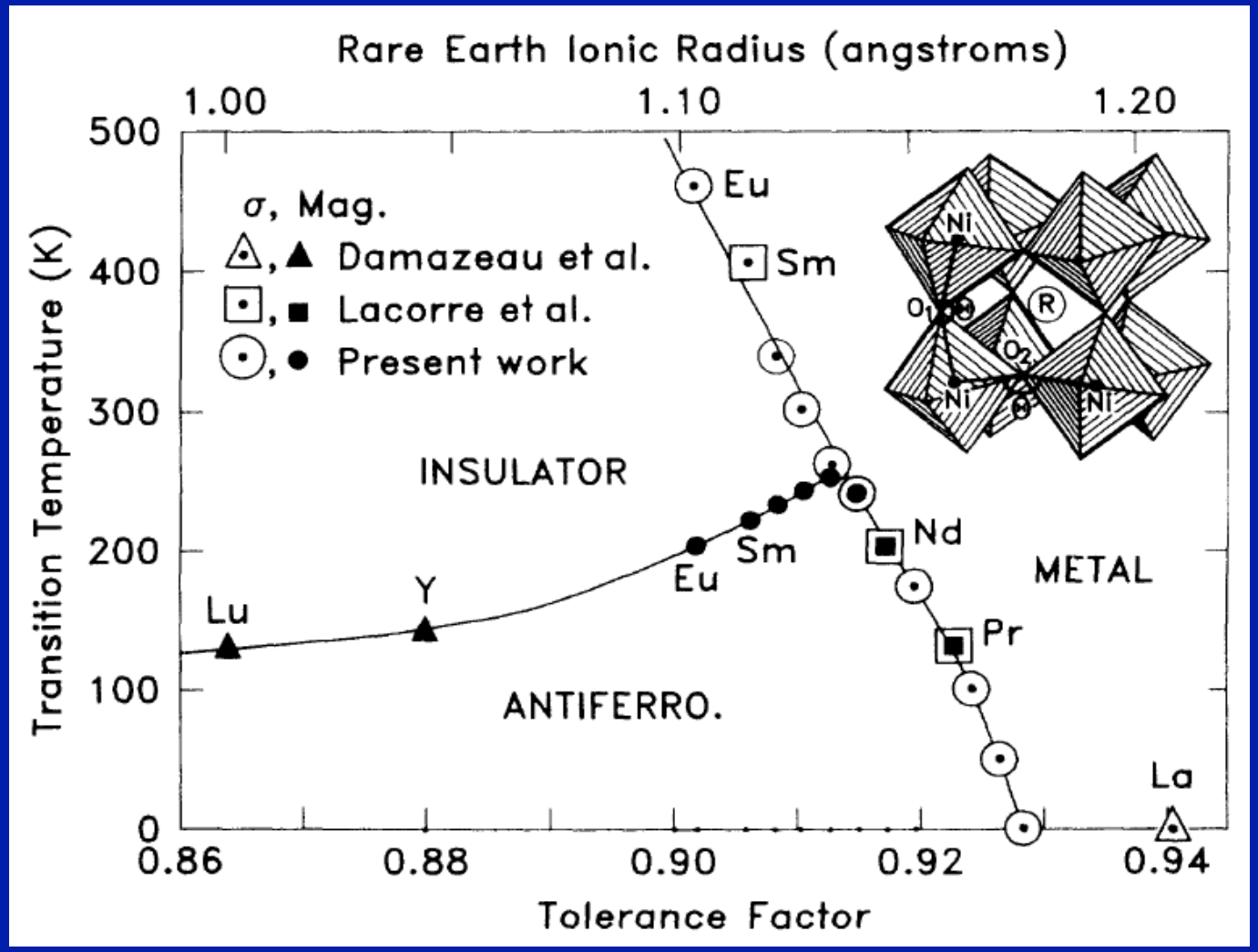

Torrance at al. Phys Rev B 45 (1992) 8209

The Mott phenomenon plays a key role

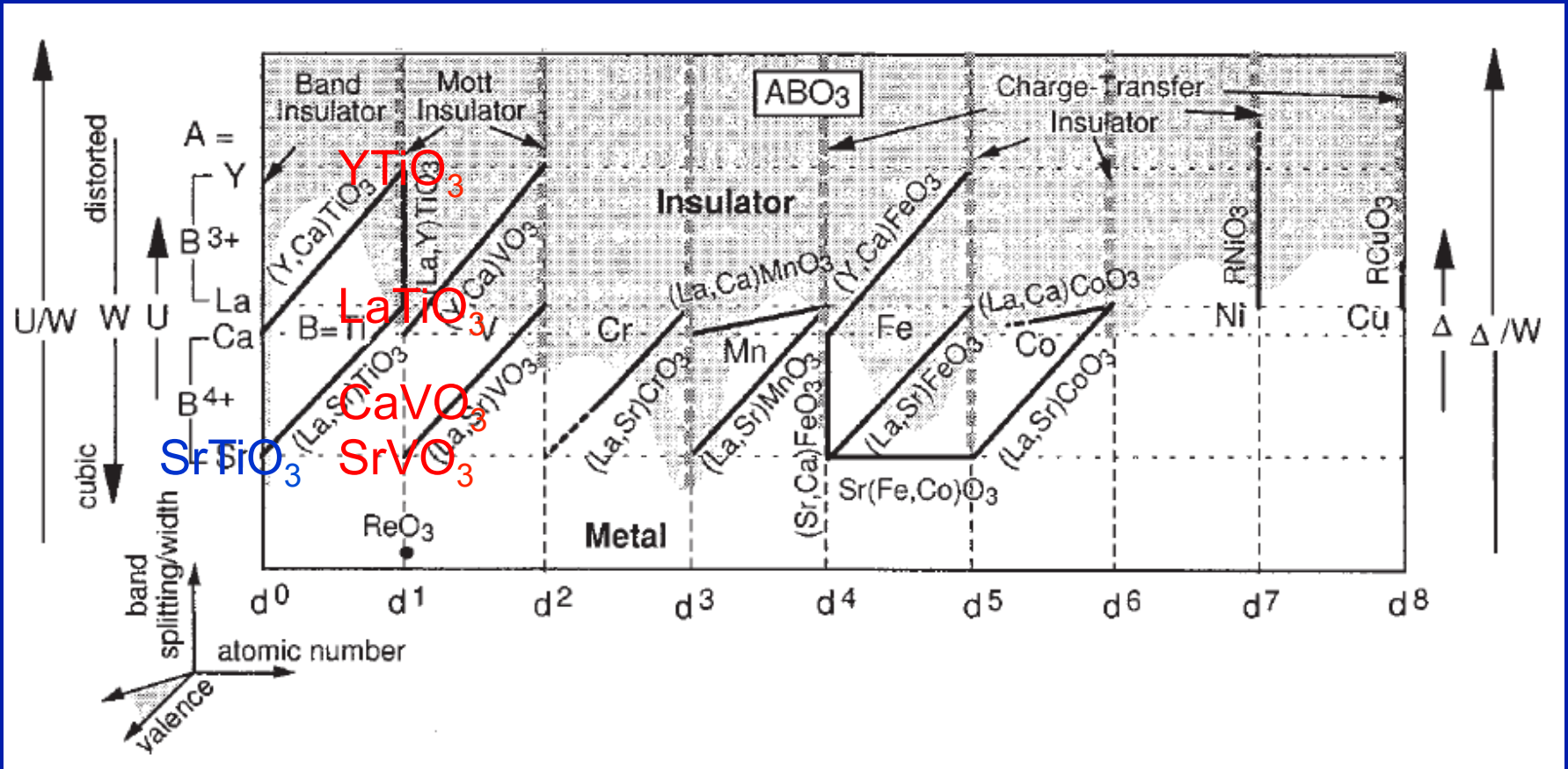

``Atsushi Fujimori's map of RMO_3 perovskites''
J.Phys Chem Sol. 53 (1992) 1595

Partially filled d-shells… and yet often insulators

Alloying on R-site changes nominal valence of M

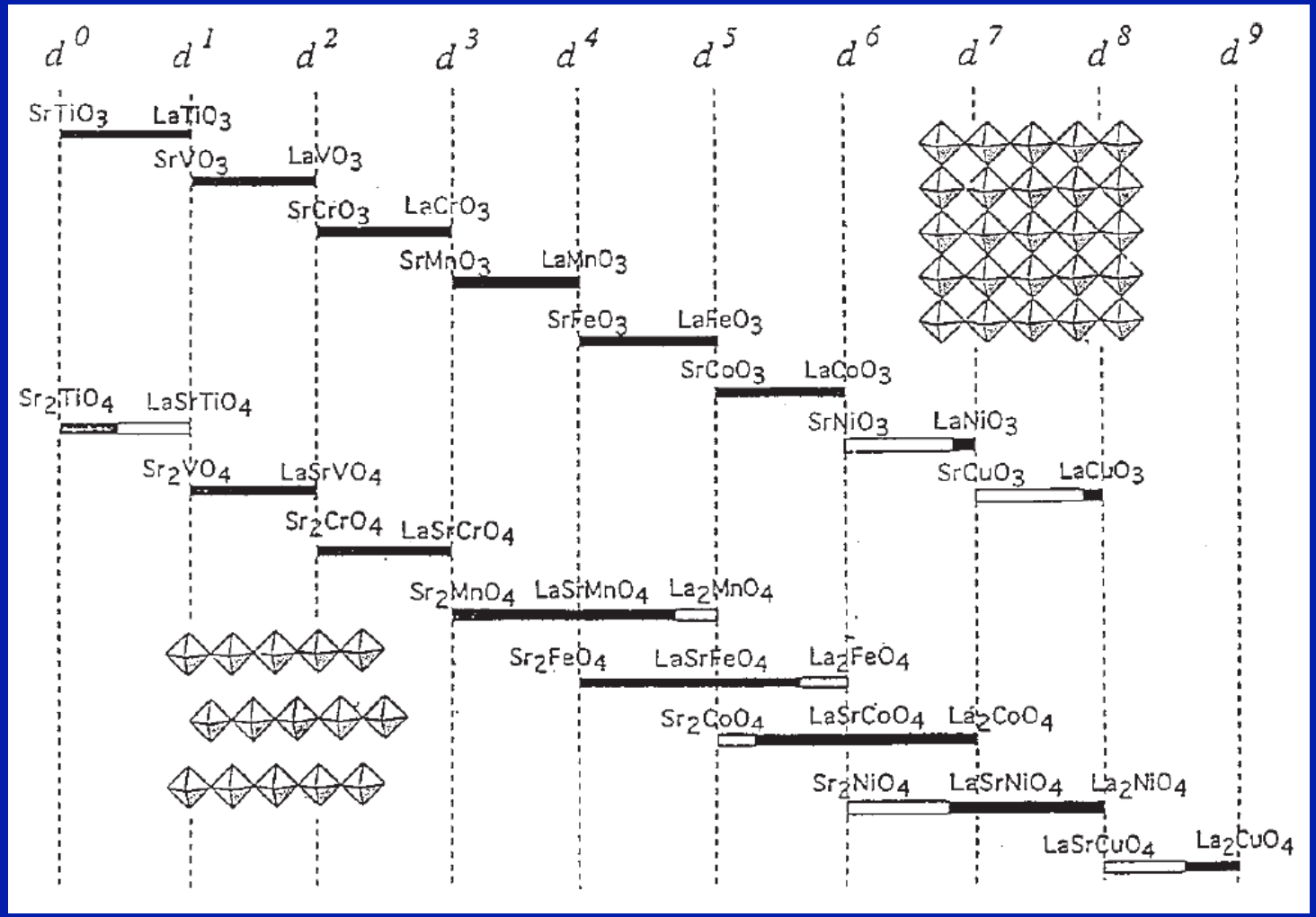

$Sr_{n+1}M_nO_{3n+1}$: 2(n+1)+4n-2(3n+1)=0 →M remains 4+ for all n

e.g. M=Ti $3d^1$ shell (titanates); M=Ru $4d^4$ shell (ruthenates)

$La_{n+1}M_nO_{3n+1}$: La^{3+} →nominal valence of M is (3n-1)/n +

e.g. La_2CuO_4 parent compound of hi-Tc SC: Cu^{2+} $3d^9$

letters to nature Nature 419, 378 (2002)

Artificial charge-modulation in atomic-scale perovskite titanate superlattices

A. Ohtomo, D. A. Muller, J. L. Grazul & H. Y. Hwang

Bell Laboratories, Lucent Technologies, Murray Hill, New Jersey 07974, USA

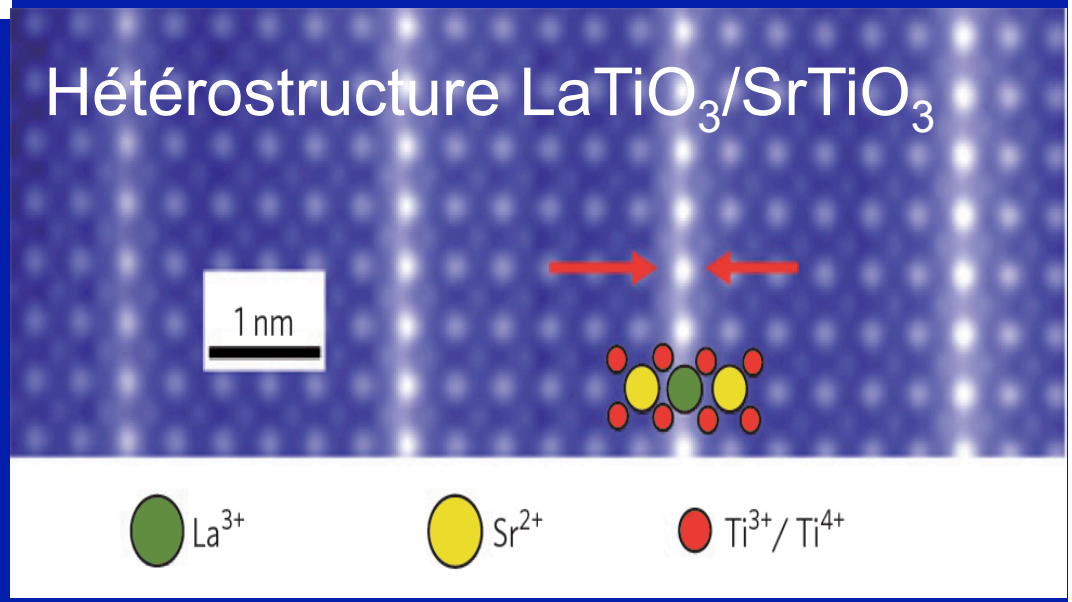

Creating a Metal out of two Insulators…

$LaTiO_3$ Mott insulator Ti^{3+} $3d^1$

/ $SrTiO_3$ band insulator Ti^{4+} $3d^0$

Engineering a new functionality by combining two (or more) materials

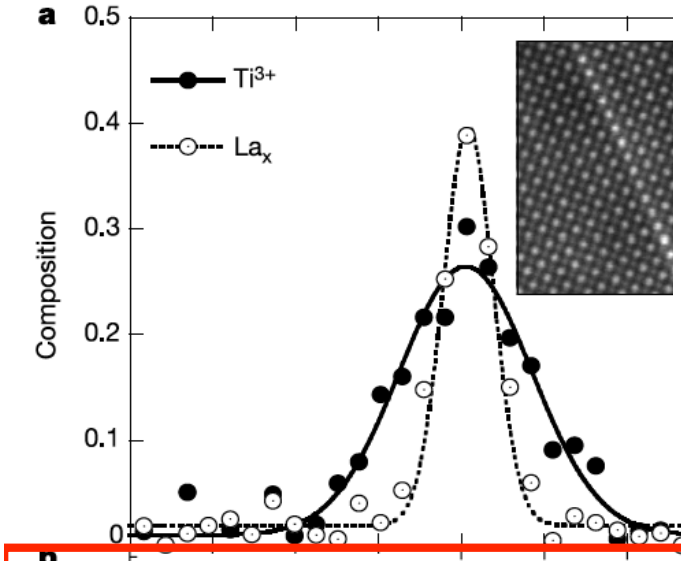

Figure 3 Spatial distribution of the Ti^{3+} signal in the vicinity of the $LaTiO_3$ layer and bilayer. **a**, EELS profiles for La and Ti recorded across a $LaTiO_3$ monolayer. Inset, the ADF image for the monolayer (layer '1' in Fig. 1). The La M edge is recorded simultaneously with the Ti L edge, yet the Ti^{3+} signal is considerably wider than that of the La. The absolute fractions of La and Ti^{3+} were calibrated from bulk $LaTiO_3$ and $SrTiO_3$. **b**, The decay of the Ti^{3+} signal away from the $LaTiO_3$ monolayer of **a** as well as the bilayer of Fig. 2. The tails of the Ti^{3+} signal for both structures fit an exponential decay with a decay length of $\lambda = 1.0 \pm 0.2$ nm.

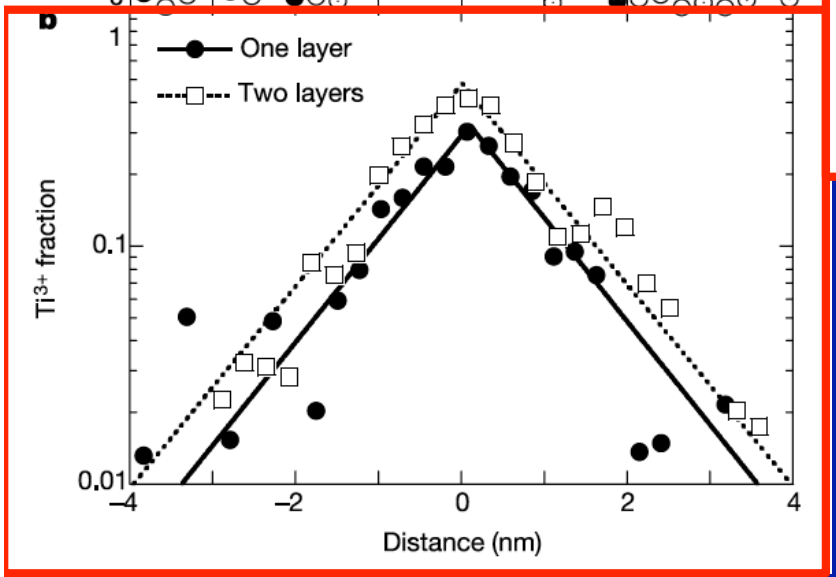

1-layer $(LTO)_1(STO)_{10}$ - EELS
Only ~ 30% of Ti in Ti^{3+} configuration

Very rapid variation over distance from interface: exponential with characteristic length ~ 1nm

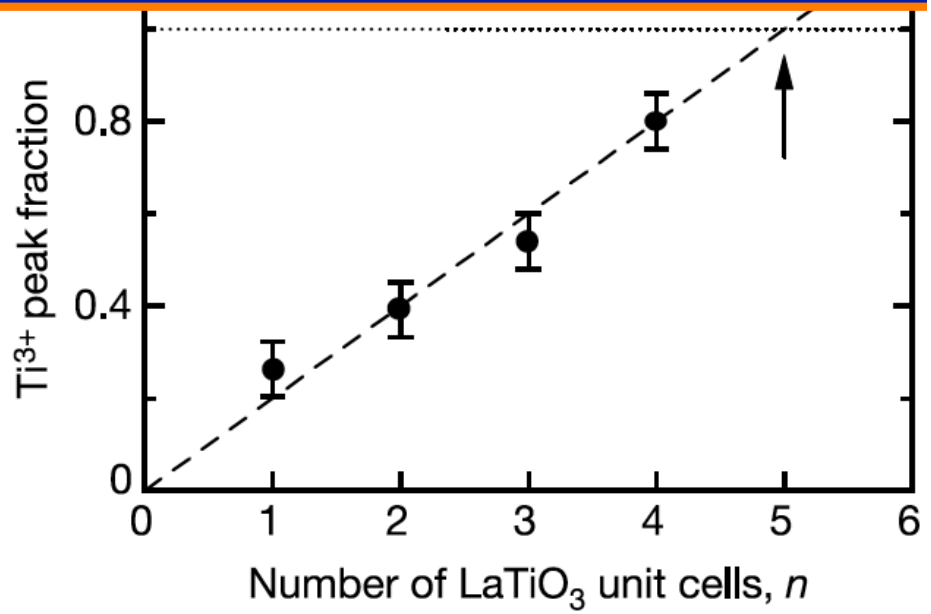

It takes about 5 layers to reach 100% of Ti in Ti^{3+} configuration, as in bulk

$(STO)_m$ $(LTO)_n$ samples are metallic, as is $La_xSr_{1-x}TiO_3$ in bulk

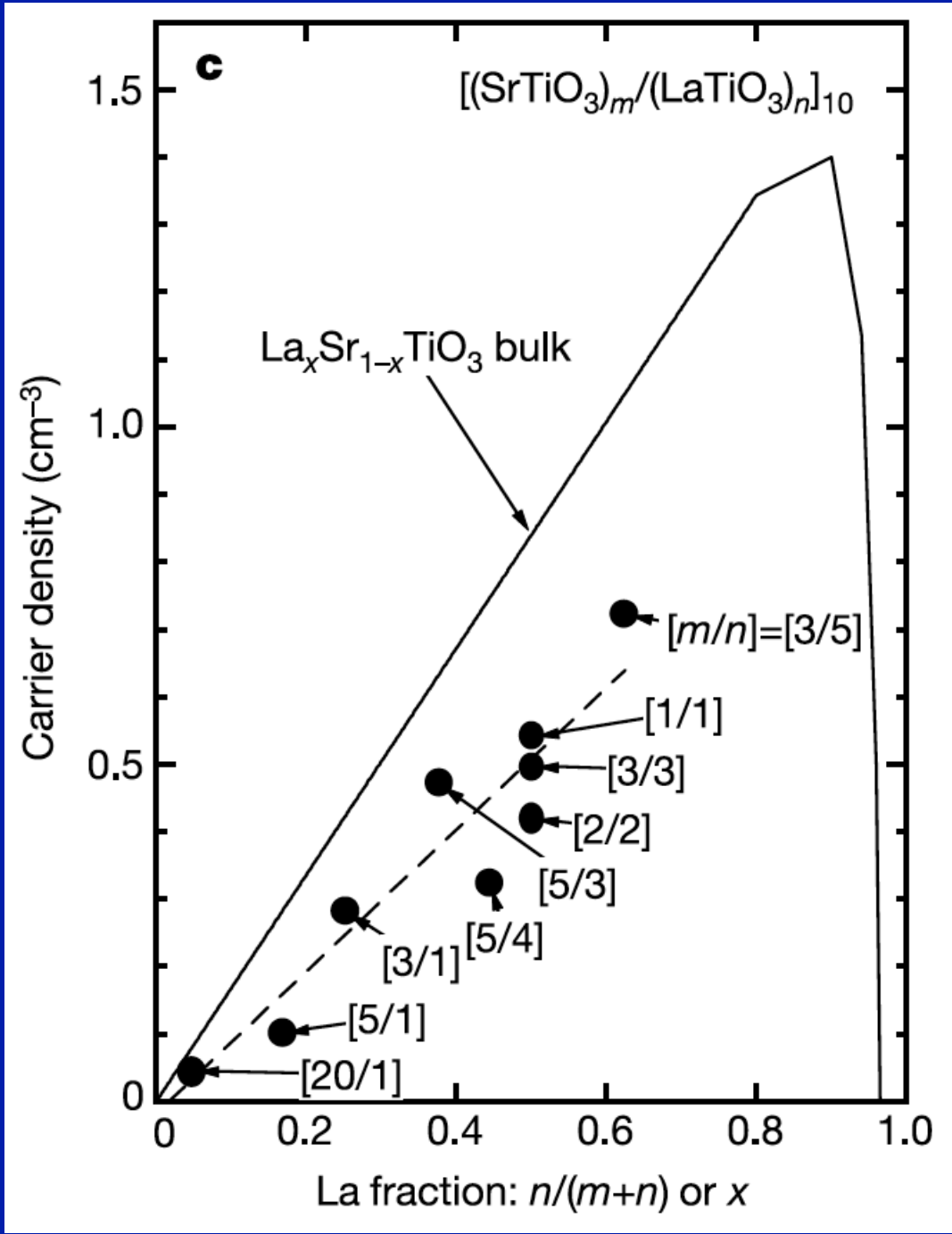

Carrier density from Hall effect

2. Crystal-Field Theory

Simple notions

(Bethe, van Vleck ~ 1930s)

How the electronic levels (of e.g. the d-shell) are split by the crystalline environment, and how this depends on the geometry and symmetry of this environment.

Orbitals: from the isolated atom to the solid
Crystal-field splitting (Bethe, van Vleck)

Cubic-symmetry adapted 3d-orbitals:

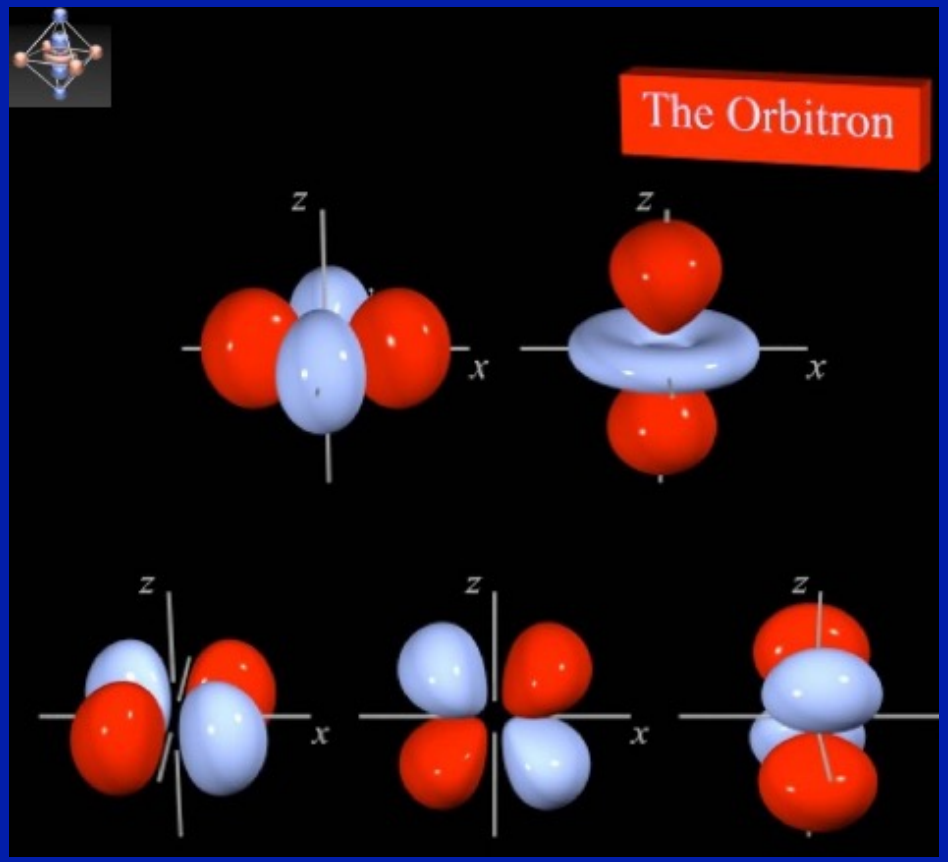

3d orbitals are quite localized:
- No nodes in radial part
- Large centrifugal barrier $l(l+1)/r^2$

$$d_{x^2-y^2}\ ,\ d_{3z^2-r^2}$$

→ The e_g doublet

$$d_{xy}\ ,\ d_{xz}\ ,\ d_{yz}$$

→ The t_{2g} triplet

http://winter.group.shef.ac.uk/orbitron

Crystal-field splitting in octahedral environment :

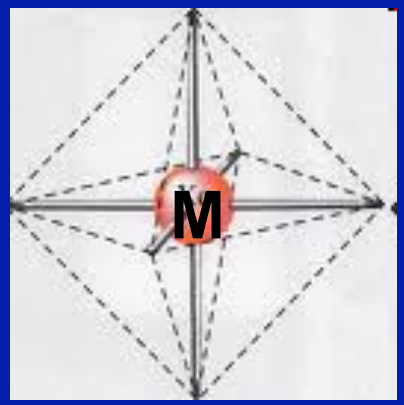

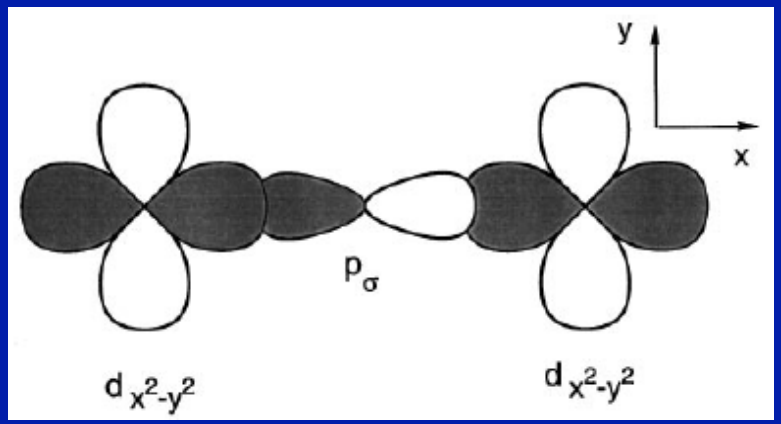

e_g orbitals point towards oxygen atoms(sigma-bonding)
→feel larger Coulomb potential
→ pushed to higher energy

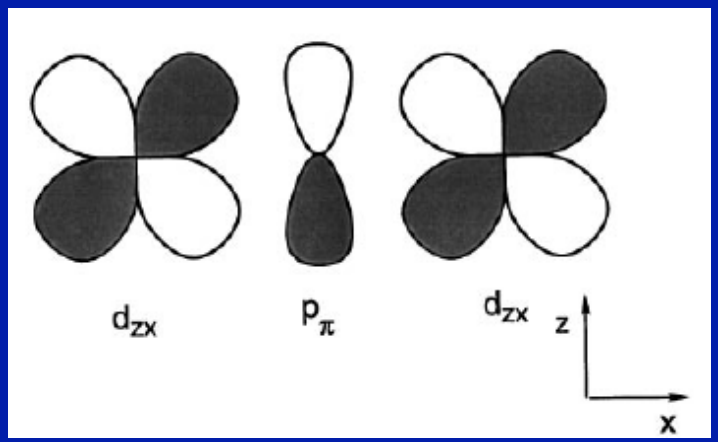

t_{2g} orbitals point away from oxygen atoms(pi-bonding)
→feel smaller Coulomb potential
→ lower energy than e_g

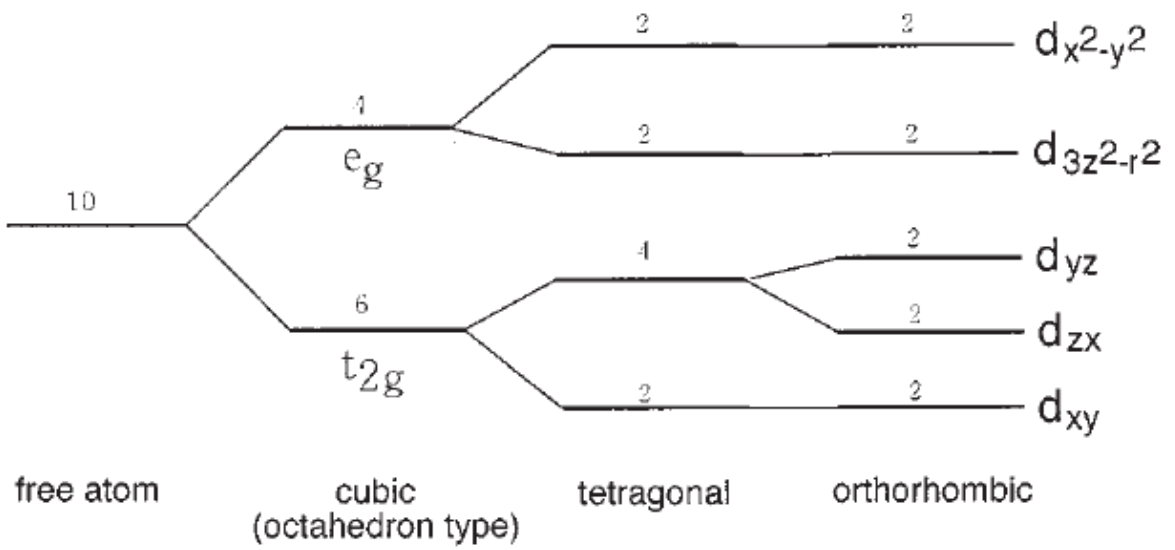

FIG. 2. Crystal-field splitting of $3d$ orbitals under cubic, tetragonal, and orthorhombic symmetries. The numbers cited near the levels are the degeneracy including spins.

Intra e_g splitting

Intra-t_{2g} splitting

Lowering further the crystal symmetry (distort from cubic)
Induces additional lifting of degeneracy

Orthohrombic perovskite → Fully lifted

Tetrahedral environment (MO_4):
e_g has lower energy, t_{2g} higher

Other environments

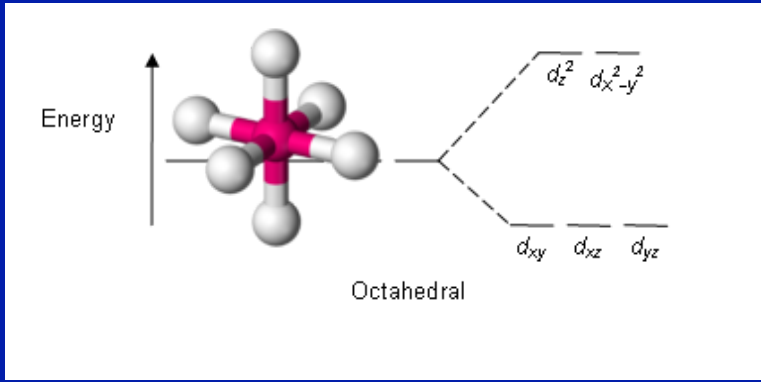

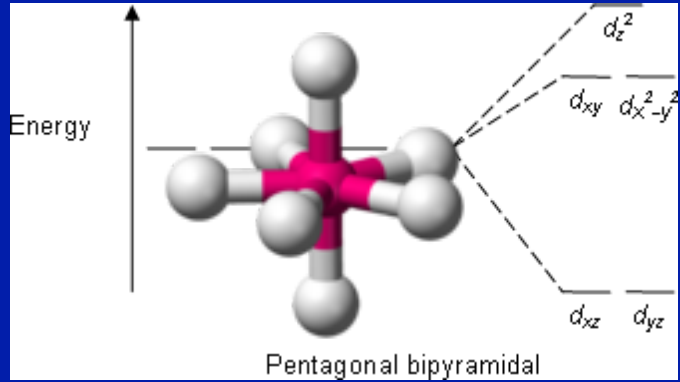

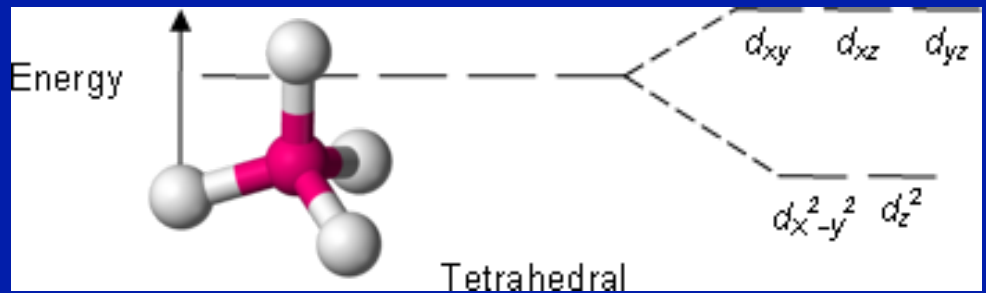

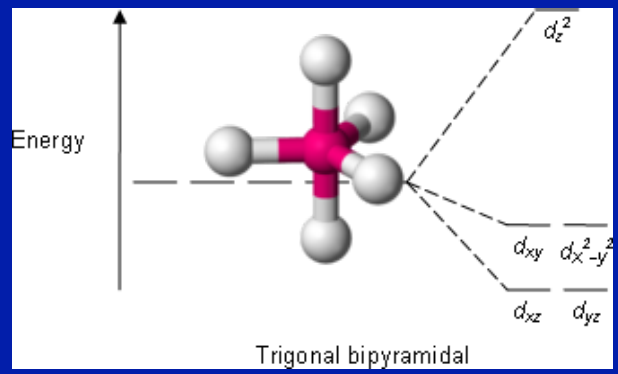

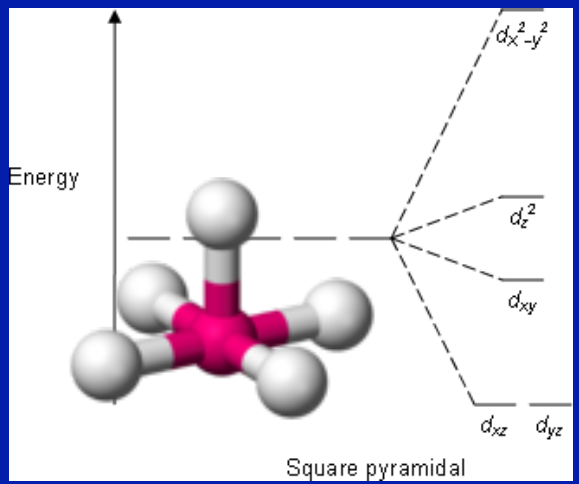

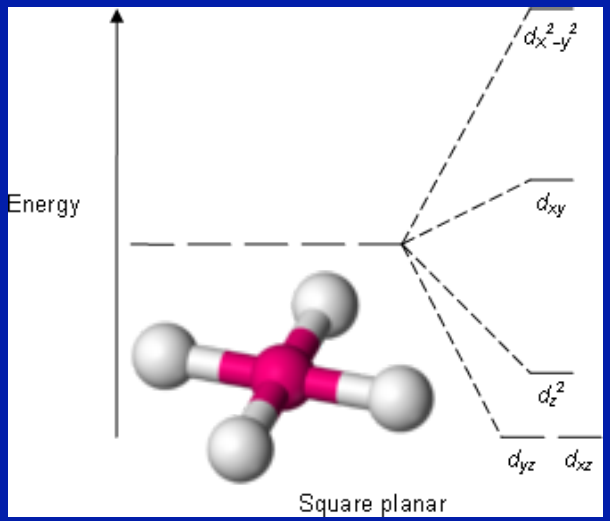

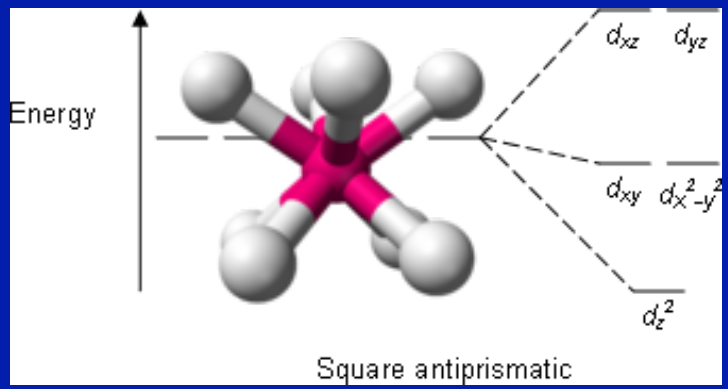

A crystal-field theory primer…

Hydrogen atom wave-functions with $l = 2$ (d-shell). Spherical coordinates: $\vec{r} = r\,(\sin\theta\cos\phi, \sin\theta\sin\phi, \cos\phi)$.

$$\psi_m(\theta,\phi) = R(r)\,Y_2^m(\theta,\phi)$$

with:

$$Y_2^0 \sim 3\cos^2\theta - 1\ ,\ Y_2^{\pm 1} \sim \sin 2\theta\, e^{\pm i\phi}\ ,\ Y_2^{\pm 2} \sim \sin^2\theta\, e^{\pm 2i\phi}$$

Cubic harmonics, transforming under irreducible representations of cubic group:

$$xy\ :\ \chi_{xy}(\theta,\phi) \sim \frac{xy}{r^2} \sim \sin\theta\cos\phi\sin\theta\sin\phi \sim \sin^2\theta\sin 2\phi \sim Y_2^{+2} - Y_2^{-2}$$

Similarly:

$$\chi_{xz} \sim Y_2^{+1} + Y_2^{-1}\ ,\ \chi_{yz} \sim Y_2^{+1} - Y_2^{-1}\ ,\ \chi_{x^2-y^2} \sim Y_2^{+2} + Y_2^{-2}\ ,\ \chi_{3z^2-r^2} \sim Y_2^0$$

MO_6 octahedron: Potential created by point charge on O-sites at center of cube, d being distance to center:

$$V(\vec{r}) \equiv \frac{Ze^2}{4\pi\varepsilon_0}\sum_{i=1}^{6}\frac{1}{||\vec{r}-\vec{R}_i||} \qquad (3.1)$$

Expand:

$$\frac{4\pi\varepsilon_0}{Ze^2}V(r) = \frac{6}{d} + \frac{7\sqrt{\pi}}{3}\frac{r^4}{d^5}\left[Y_4^0(\theta,\phi) + \sqrt{\frac{5}{14}}(Y_4^4(\theta,\phi) + Y_4^{-4}(\theta,\phi))\right] + \cdots \tag{3.2}$$

Treat second term as perturbation $\delta V(r,\theta,\phi)$: breaks spherical symmetry. Because of proper choice of cubic orbital above:

$$\begin{aligned}\langle\chi_m|\delta V|\chi_{m'}\rangle &= \Delta_t\,\delta_{mm'} \text{ for } m = xy, xz, yz \\ &= \Delta_e\,\delta_{mm'} \text{ for } m = x^2 - y^2, 3z^2 - r^2\end{aligned}$$

with:

$$\boxed{\Delta_e - \Delta_t = 1.67\,\frac{Ze^2}{4\pi\varepsilon_0\,d^5}\int_0^\infty r^4 R(r)^2\,r^2 dr \equiv \text{“}10Dq\text{”}}$$

Why do we care about energies of crystal-field level ?

- Which levels get occupied determines electronic configuration, hence crucial for physics and chemistry
- Low-spin vs. High-spin, Optical properties etc…
- Criterion determining whether a material is a metal or Mott insulator <u>crucially dependent on energy splitting between levels/lifting of degeneracy of d-shell and subshells</u>.

Why is ruby red ?

cf e.g: http://www.chm.davidson.edu/vce/CoordChem/CFT.html

Ruby: small amount Of Cr^{3+} impurities Substituting Al^{3+} in Al_2O_3 (corundom), a large-gap transparent insulator

Cr3+ ($3d^3$) 3 electrons in t_{2g} shell

$$\Delta_0 = 2.21\,\mathrm{eV} \rightarrow \lambda \simeq 561\,\mathrm{nm}$$

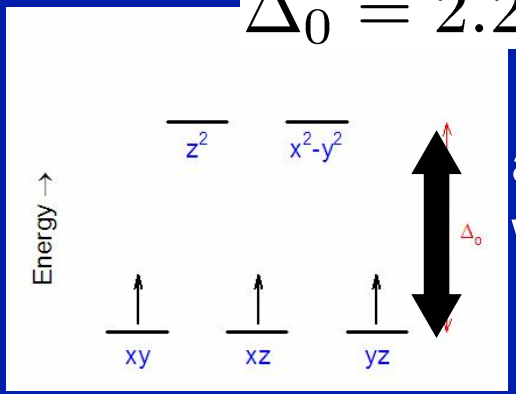

absorption of most visible wavelength beyond red

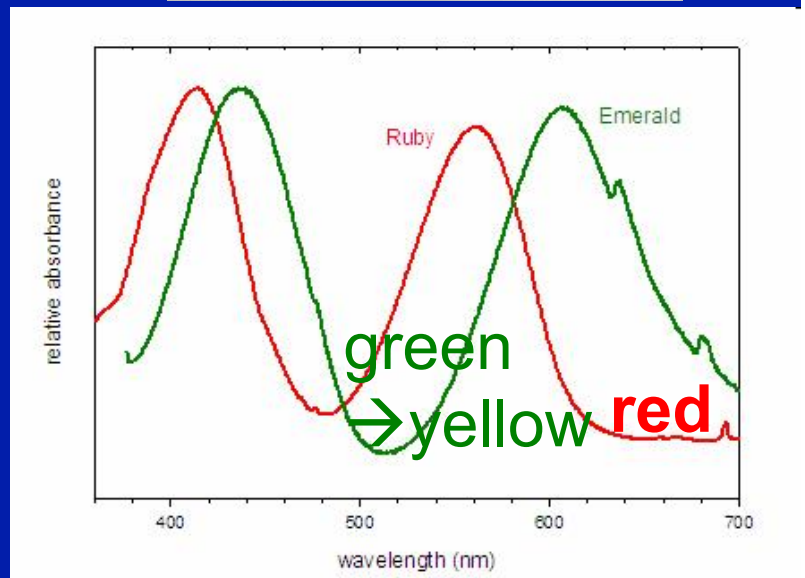

Dependence on Mott critical U/W on the number of orbitals

x electrons in N orbitals
(filling x/2N)
Gutzwiller approximation
J.P. Lu Phys
Rev B 49 (1994) 5687

$$U_c(N,x) = \frac{[\sqrt{x(2N-x+1)}+\sqrt{(x+1)(2N-x)}]^2}{2N-x}|\bar{\epsilon}(x)|$$

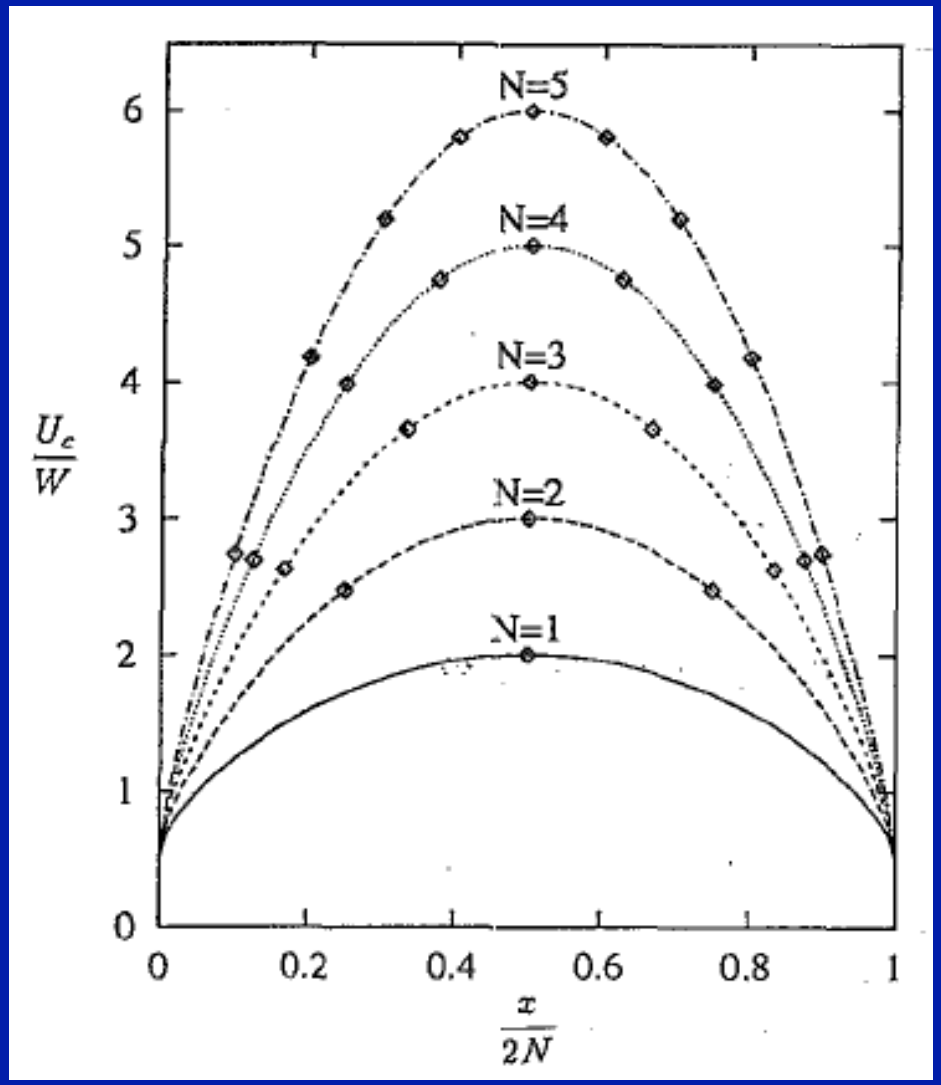

Note: this dependence on filling is unphysical, due to the neglect of the Hund's coupling. In reality, the ½-filled shell has the SMALLEST Uc

4. More on distortions of perovskites
(In the bulk and in thin films and heterostructures)

- Discussions gratefully acknowledged with:
- Jean-Marc Triscone, Jennifer Fowlie (Geneva)
- Claude Ederer, Alex Hampel (ETH-Zurich)

Different types of distortions

- Tilts and Rotations of Octahedra
- Deformation of the local octahedral shape: Jahn-Teller distortion (often appearing when electronic configuration is degenerate, such as to lift degeneracy)
- Off-centering of Metal (B-cation) → Ferroelectric distortion
- Other distortion patterns: breathing mode cf. Nickelates lectures 3-4

Tilts and Rotations
- Introduction to Glazer notations

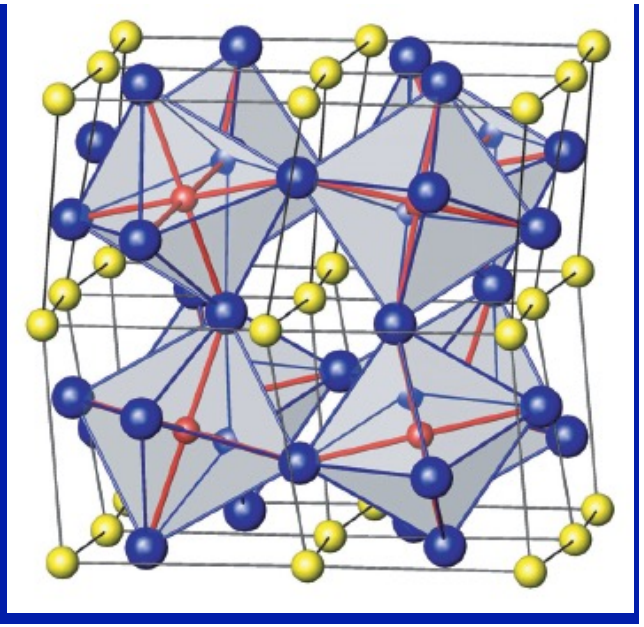

Acta Cryst. (1972). B**28**, 3384

The Classification of Tilted Octahedra in Perovskites

BY A. M. GLAZER

Crystallographic Laboratory, Cavendish Laboratory, Cambridge, England

(*Received* 4 *May* 1972)

A simple method for describing and classifying octahedral tilting in perovskites is given and it is shown how the tilts are related to the unit-cell geometries. Several examples from the literature are listed and predictions about hitherto unknown structures of some materials are made.

Glazer,Acta Cryst (1972) B28,3384; (1975) A31, 756
Woodward, Acta Cryst (1997) B53, 32 ; Howard Acta Cryst B54 (1998) 782

Use Rotation angles about axis of (pseudo-)cubic structure:

a [100] → α , b[010]→β , c[001]→γ

Glazer notations:

aaa = equal rotation angle about all three axes (α=β=γ)

aac → α=β ≠ γ

abc → αβγ all different

etc.

Upper +/- index:

+: octahedra along a given axis are rotated in-phase about this axis

-: they are rotated out of phase

0: no tilt.

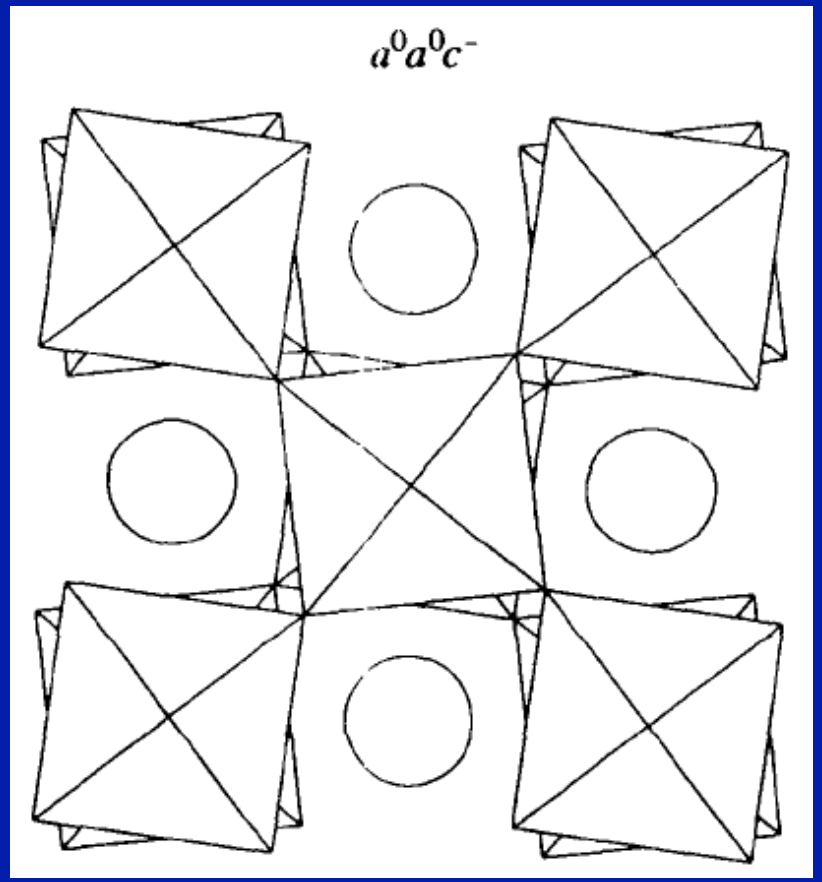

Ex: $a^0a^0c^-$ seen along c-axis

Tilts/ Rotations double the unit cell

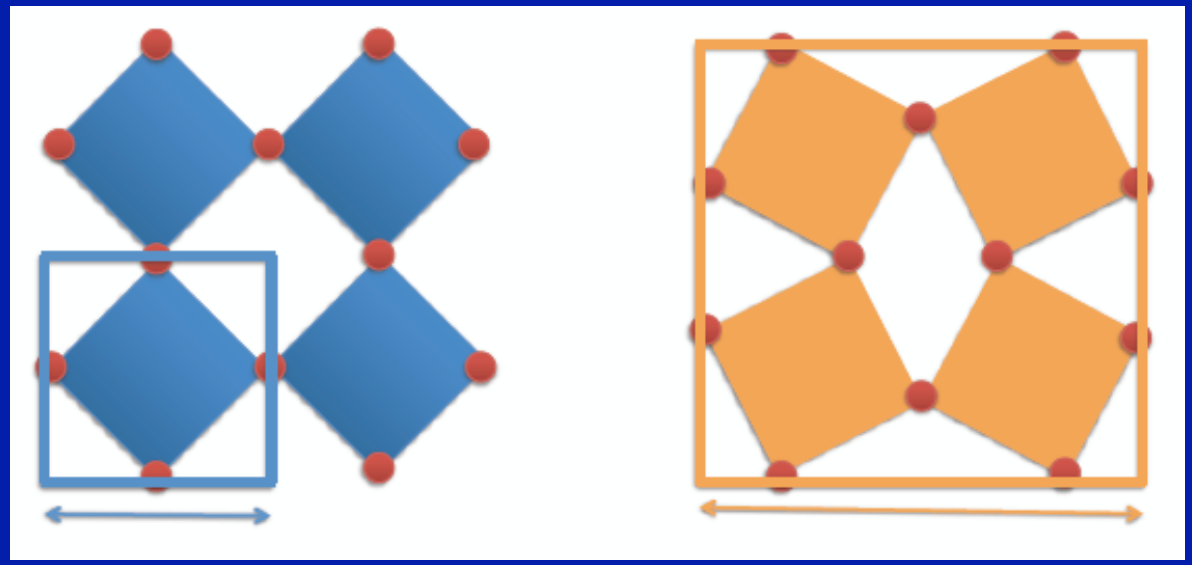

This leads to new Bragg peaks with ½-integer h,k,l in X-ray diffraction
→ analysis of form factor allows to identify/quantify rotations.
cf. May et al.
Phys Rev B 82 (2010) 014110

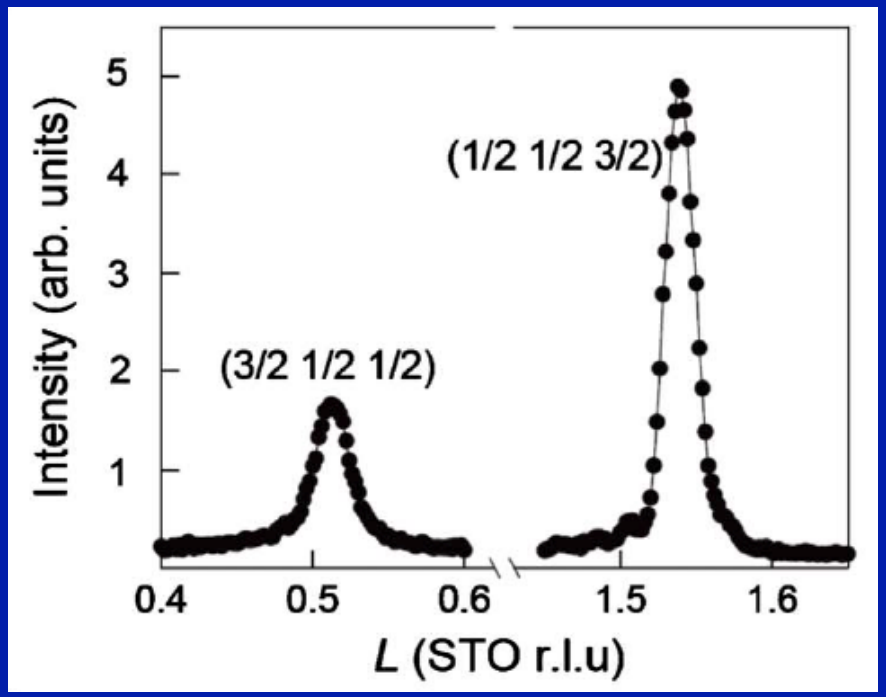

LaNiO3 on SrTiO3

Tilts/Rotations lower the symmetry

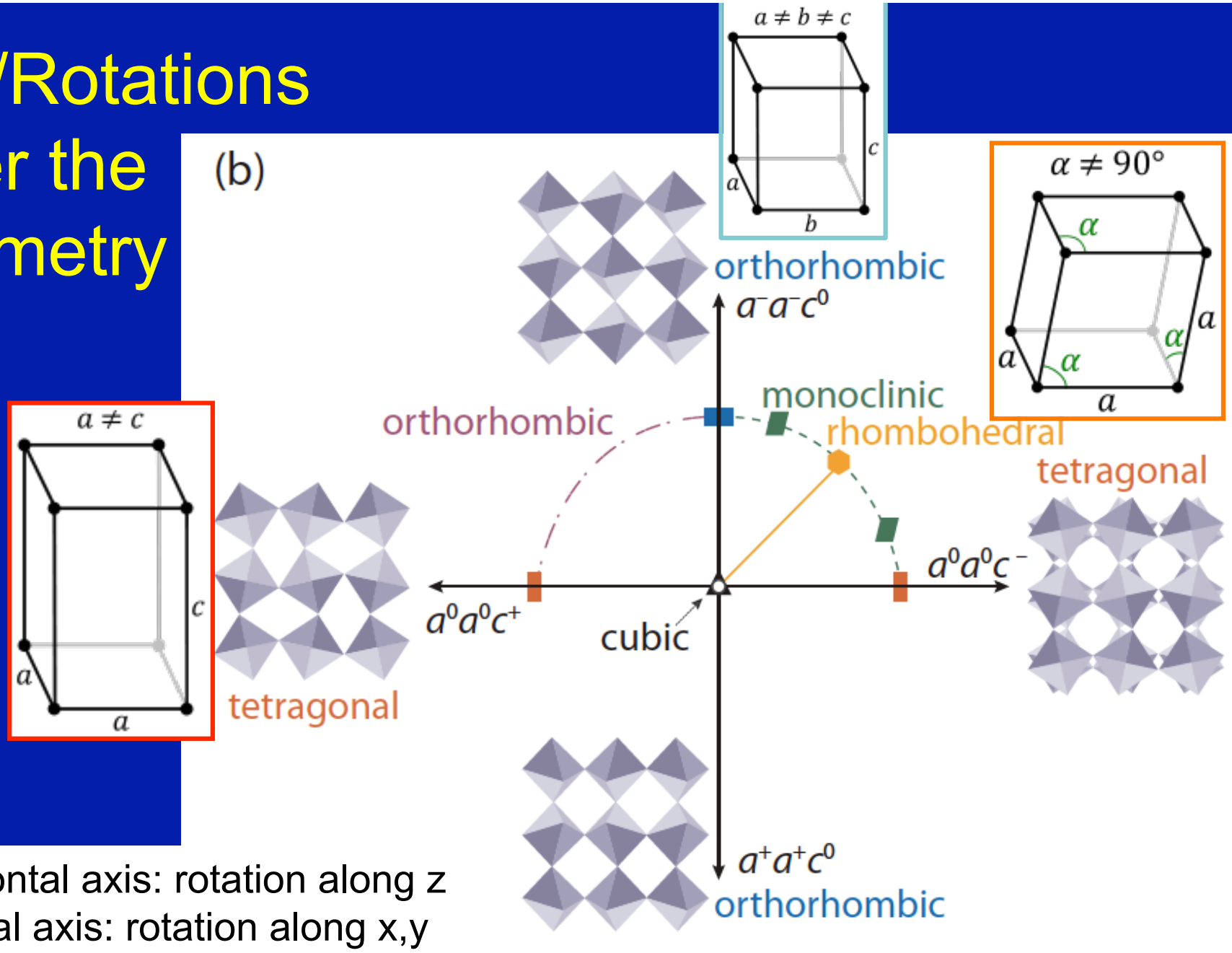

Horizontal axis: rotation along z
Vertical axis: rotation along x,y

Rondinelli and Spaldin, Adv. Mater. 23 (2011) 3363

Table 1. *Complete list of possible simple tilt systems*

Serial number	Symbol	Lattice centring	Multiple cell	Relative pseudocubic subcell parameters	Space group
Three-tilt systems					
(1)	$\mathbf{a}^+\mathbf{b}^+\mathbf{c}^+$	I	$2a_p \times 2b_p \times 2c_p$	$a_p \neq b_p \neq c_p$	$Immm$ (No. 71)
(2)	$\mathbf{a}^+\mathbf{b}^+\mathbf{b}^+$	I		$a_p \neq b_p = c_p$	$Immm$ (No. 71)
(3)	$\mathbf{a}^+\mathbf{a}^+\mathbf{a}^+$	I		$a_p = b_p = c_p$	$Im3$ (No. 204)
(4)	$\mathbf{a}^+\mathbf{b}^+\mathbf{c}^-$	P		$a_p \neq b_p \neq c_p$	$Pmmn$ (No. 59)
(5)	$\mathbf{a}^+\mathbf{a}^+\mathbf{c}^-$	P		$a_p = b_p \neq c_p$	$Pmmn$ (No. 59)
(6)	$\mathbf{a}^+\mathbf{b}^+\mathbf{b}^-$	P		$a_p \neq b_p = c_p$	$Pmmn$ (No. 59)
(7)	$\mathbf{a}^+\mathbf{a}^+\mathbf{a}^-$	P		$a_p = b_p = c_p$	$Pmmn$ (No. 59)
(8)	$\mathbf{a}^+\mathbf{b}^-\mathbf{c}^-$	A		$a_p \neq b_p \neq c_p$ $\alpha \neq 90°$	$A2_1/m11$ (No. 11)
(9)	$\mathbf{a}^+\mathbf{a}^-\mathbf{c}^-$	A		$a_p = b_p \neq c_p$ $\alpha \neq 90°$	$A2_1/m11$ (No. 11)
(10)	$\mathbf{a}^+\mathbf{b}^-\mathbf{b}^-$	A		$a_p \neq b_p = c_p$ $\alpha \neq 90°$	$Pmnb$ (No. 62)*†
(11)	$\mathbf{a}^+\mathbf{a}^-\mathbf{a}^-$	A		$a_p = b_p = c_p$ $\alpha \neq 90°$	$Pmnb$ (No. 62)*†
(12)	$\mathbf{a}^-\mathbf{b}^-\mathbf{c}^-$	F		$a_p \neq b_p \neq c_p$ $\alpha \neq \beta \neq \gamma \neq 90°$	$F\bar{1}$ (No. 2)
(13)	$\mathbf{a}^-\mathbf{b}^-\mathbf{b}^-$	F		$a_p \neq b_p = c_p$ $\alpha \neq \beta \neq \gamma \neq 90°$	$I2/a$ (No. 15)*
(14)	$\mathbf{a}^-\mathbf{a}^-\mathbf{a}^-$	F		$a_p = b_p = c_p$ $\alpha = \beta = \gamma \neq 90°$	$R\bar{3}c$ (No. 167)
Two-tilt systems					
(15)	$\mathbf{a}^0\mathbf{b}^+\mathbf{c}^+$	I	$2a_p \times 2b_p \times 2c_p$	$a_p < b_p \neq c_p$	$Immm$ (No. 71)
(16)	$\mathbf{a}^0\mathbf{b}^+\mathbf{b}^+$	I		$a_p < b_p = c_p$	$I4/mmm$ (No. 139)†
(17)	$\mathbf{a}^0\mathbf{b}^+\mathbf{c}^-$	B		$a_p < b_p \neq c_p$	$Bmmb$ (No. 63)
(18)	$\mathbf{a}^0\mathbf{b}^+\mathbf{b}^-$	B		$a_p < b_p = c_p$	$Bmmb$ (No. 63)
(19)	$\mathbf{a}^0\mathbf{b}^-\mathbf{c}^-$	F		$a_p < b_p \neq c_p$ $\alpha \neq 90°$	$F2/m11$ (No. 12)
(20)	$\mathbf{a}^0\mathbf{b}^-\mathbf{b}^-$	F		$a_p < b_p = c_p$ $\alpha \neq 90°$	$Imcm$ (No. 74)*
One-tilt systems					
(21)	$\mathbf{a}^0\mathbf{a}^0\mathbf{c}^+$	C	$2a_p \times 2b_p \times c_p$	$a_p = b_p < c_p$	$C4/mmb$ (No. 127)
(22)	$\mathbf{a}^0\mathbf{a}^0\mathbf{c}^-$	F	$2a_p \times 2b_p \times 2c_p$	$a_p = b_p < c_p$	$F4/mmc$ (No. 140)
Zero-tilt system					
(23)	$\mathbf{a}^0\mathbf{a}^0\mathbf{a}^0$	P	$a_p \times b_p \times c_p$	$a_p = b_p = c_p$	$Pm3m$ (No. 221)

23 tilt systems and corresponding symmetry group

(See: Glazer 1975, Woodward 1998 – op. cit.)

Only 15 of them can actually be realized ?

see Howard and Stokes Acta Cryst (1998) B54 782

How Strain (controlled by choice of substrate in thin films) influences Tilts/Rotations

- Given the difficulty of determining experimentally oxygen positions accurately (see today's seminar: STEM, EELS), electronic structure calculations (DFT and beyond) are particularly useful here.
- See in particular: J.Rondinelli and N.Spaldin Adv. Mater. 23 (2011) 3363; May et al. Phys Rev B 82 (2010) 014110; Peil et al Phys Rev B 90, 045128 (2014)

Accommodating strain…

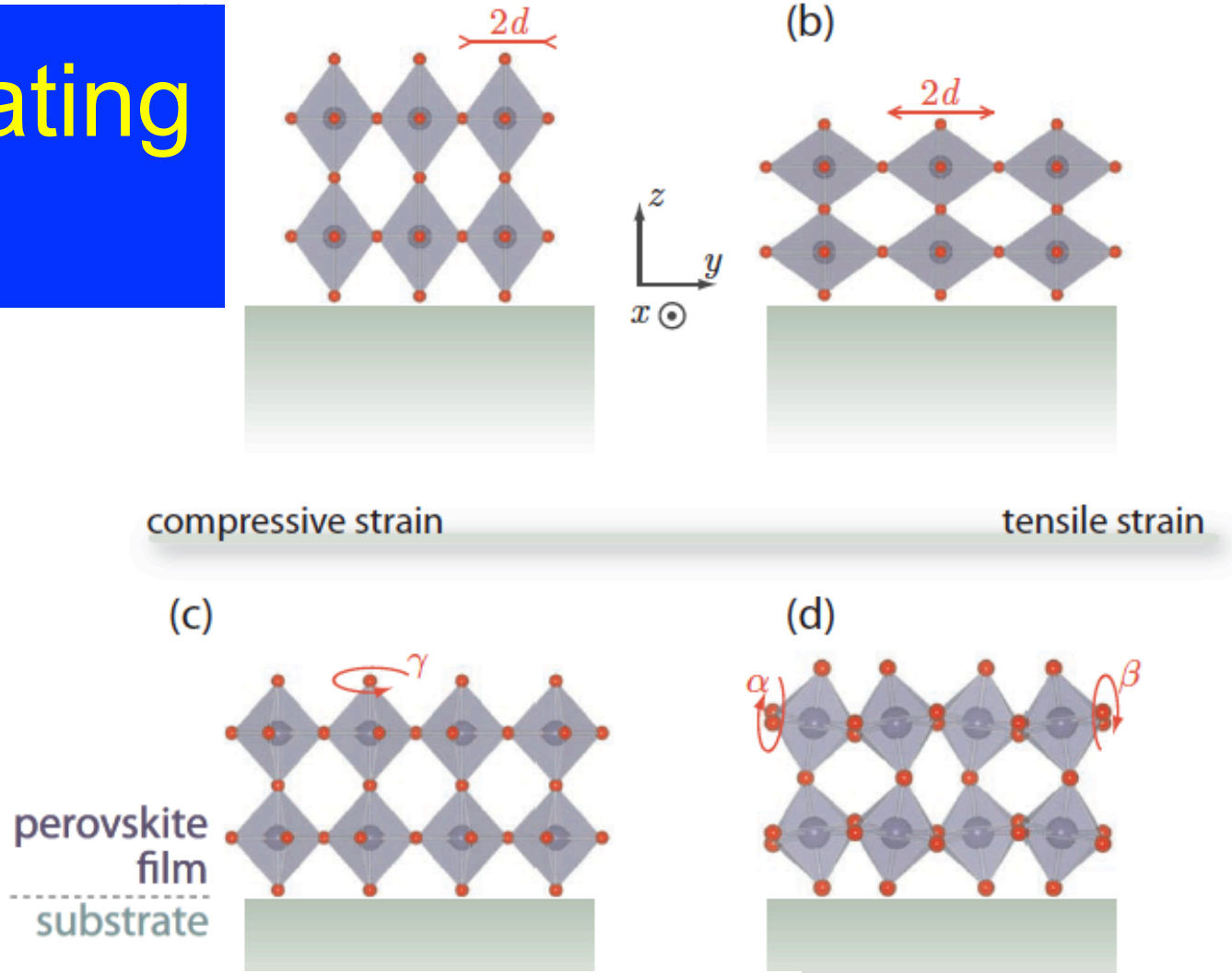

Figure 3. In coherently strained perovskite films, the BO_6 octahedra can distort through contraction (a) or elongation (b) of the equatorial *B*–O bond lengths *d* due to compressive or tensile strain, respectively. Simultaneously or alternatively, the octahedra can accommodate the substrate-induced change of the in-plane lattice parameters by rotation perpendicular to the substrate as in (c), and/or about an axis parallel to the substrate plane (d).

Example: Strained $LaNiO_3$

Peil, Ferrero and Georges Phys Rev B 90, 045128 (2014)
see also:May et al. Phys Rev B 82, 014110 (2010)

Biaxial strain: $\epsilon = a/a_{eq} - 1$

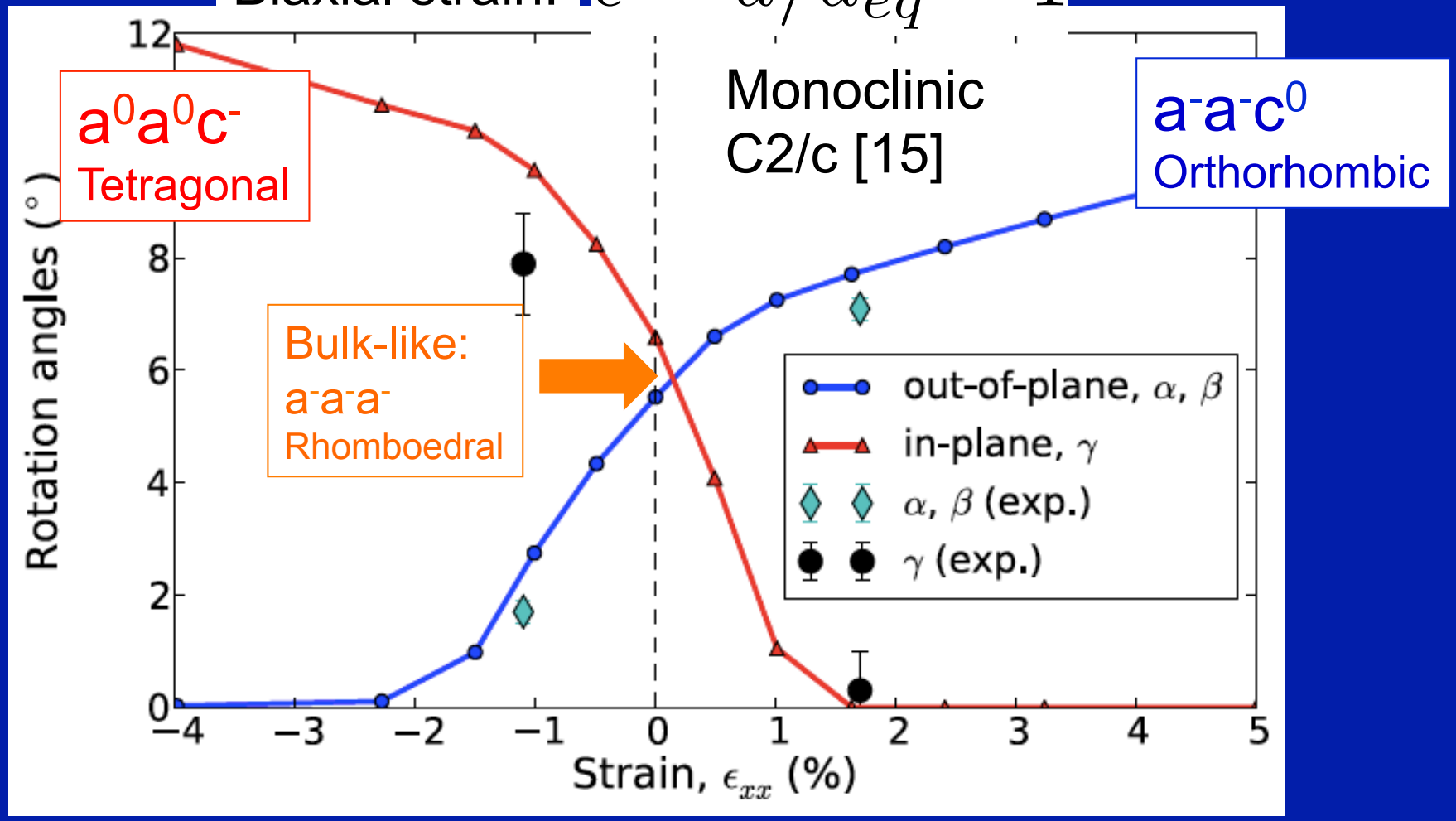

Commonly used substrates

Table 2. Lattice parameters, crystal structures and tilt systems of common substrate materials used in oxide thin film growth. Pseudo-cubic lattice parameters are given in parentheses. For rhombohedral space groups $a_{pc} \sim a/\sqrt{2}$. For orthorhombic substrates values in parentheses correspond to the average pseudocubic spacing $[\sqrt{(a^2+b^2)}/2]$ along the [110] direction.

Substrate	Structure	Temperature [K]	Tilt System	Lattice constants [Å]	Reference
SrTiO3 (STO)	Cubic (221, $Pm\bar{3}m$)	>105	$a^0a^0a^0$	$a = 3.905$	[181]
	Tetragonal (140, $I4/mcm$)	<105	$a^0a^0c^-$	$c/a = 1.0056$	
$LaAlO_3$ (LAO)	Cubic (221, $Pm\bar{3}m$)	>800	$a^0a^0a^0$	$a = 3.81$	[182]
	Rhombohedral (167, $R\bar{3}c$)	<800	$a^-a^-a^-$	$a = 5.36$ (3.79)	[183]
LSAT	Cubic (221, $Pm\bar{3}m$)	>150	$a^0a^0a^0$	$a = 3.87$	[184]
	Tetragonal (140, $I4/mcm$)	<150	$a^0a^0c^-$	$a = 5.46$ (3.86), $c = 7.73$ (3.87)	
$LaGaO_3$ (LGO)	Rhombohedral (167, $R\bar{3}c$)	>420	$a^-a^-a^-$	$a = 5.58$ (3.94)	[185]
	Orthorhombic (62, $Pnma$)	<420	$a^+b^-b^-$	$a = 5.49$, $b = 5.53$; (3.90), $c = 7.78$ (3.89)	[186]
$DyScO_3$ (DSO)	Orthorhombic (62, $Pnma$)		$a^+b^-b^-$	$a = 5.44$, $b = 5.53$; (3.88), $c = 7.89$ (3.95)	[187]

From:
J.Rondinelli and N.Spaldin
Adv. Mater. 23 (2011) 3363

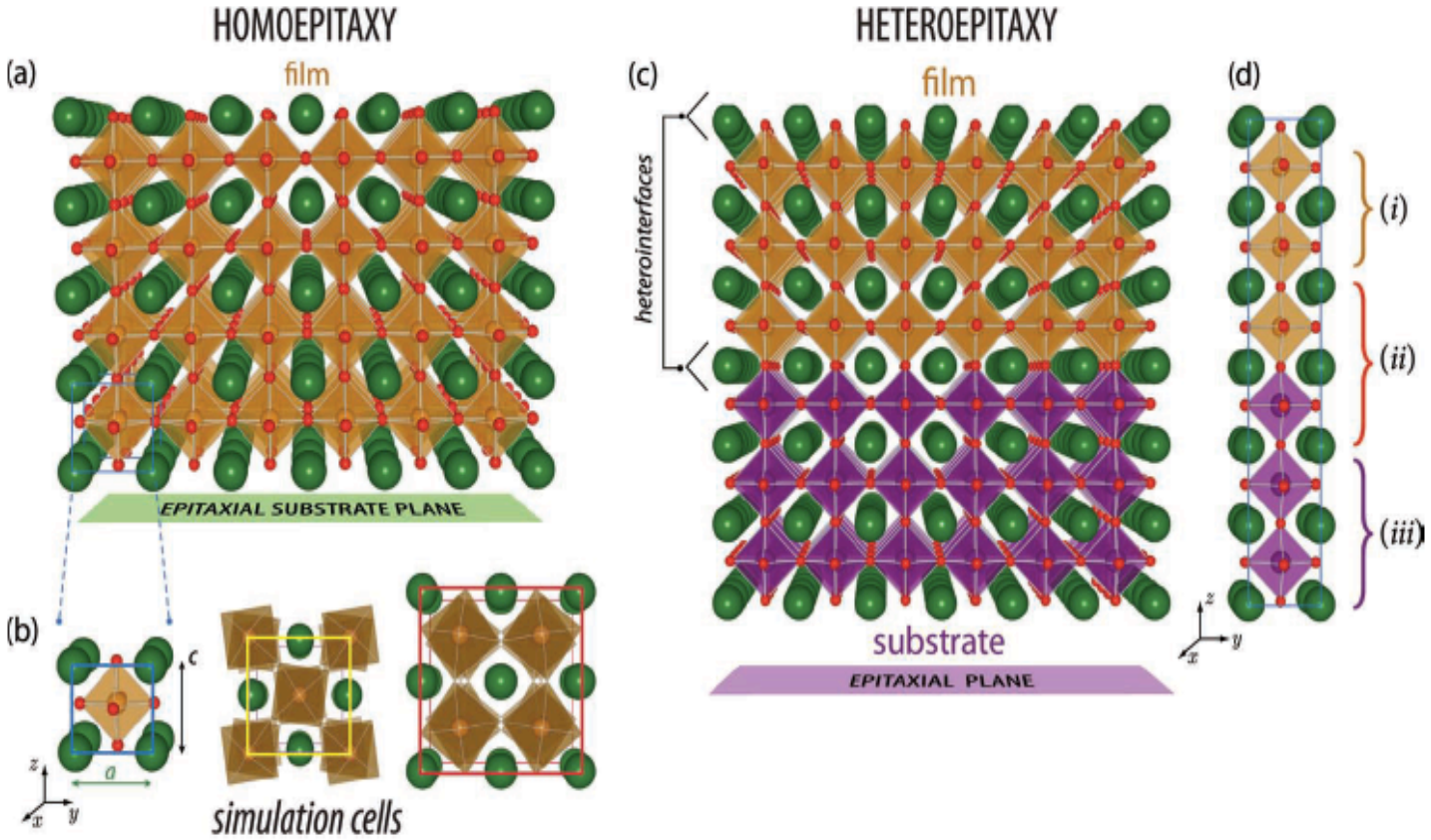

Figure 4. Illustration of the homoepitaxial and heteroepitaxial strain models. Possible choices for the fundamental unit cell used to represent the homoepitaxial film (a) in a periodic boundary condition DFT-calculation are shown in (b). The left cartoon shows a primitive 5-atom perovskite unit cell, and $\sqrt{2} \times \sqrt{2} \times 2$ and $2 \times 2 \times 2$ supercells are shown center and right. The particular cell size is selected in order to accommodate arrangements of various structural and electronic internal degrees freedom. In the heteroepitaxial strain calculations, the substrate and film are both present in the primitive heterostructure cell (d).

DFT calculations: without and with explicit inclusion of the substrate [Rondinelli-Spaldin, Adv. Mater, op. cit.]

Imaging octahedral distortions in thin films and heterostructures

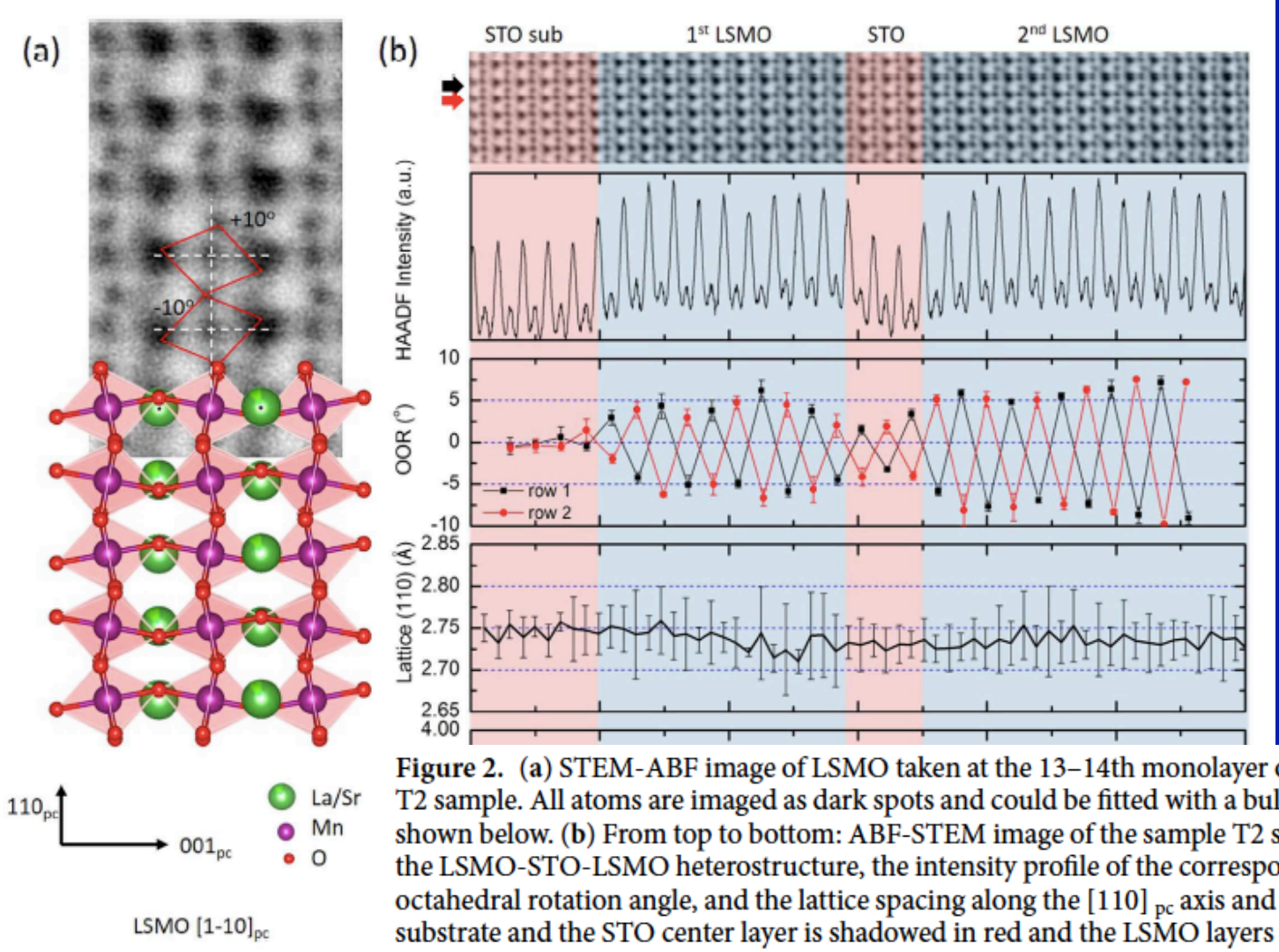

Figure 2. (a) STEM-ABF image of LSMO taken at the 13–14th monolayer of the top LSMO layer of the trilayer T2 sample. All atoms are imaged as dark spots and could be fitted with a bulk-like LSMO structure model shown below. (b) From top to bottom: ABF-STEM image of the sample T2 showing both the STO substrate and the LSMO-STO-LSMO heterostructure, the intensity profile of the corresponding HAADF image, the oxygen octahedral rotation angle, and the lattice spacing along the $[110]_{pc}$ axis and the out-of-plane *c* axis. The STO substrate and the STO center layer is shadowed in red and the LSMO layers are shadowed in blue. The line profiles are the average values of all atomic rows presented in the ABF image and the error bars are the standard deviation using the formulation $\sqrt{\frac{\sum(x-\bar{x})^2}{(n-1)}}$.

Li et al. Scientific Reports doi:10.1038/srep40068

5.From Crystal-Field Theory to Band Structure

… to be continued in Lecture 3